A Boolean network model of hypoxia, mechanosensing and TGF-β signaling captures the role of phenotypic plasticity and mutations in tumor metastasis

Short title:

Boolean model of hypoxia, mechanosensing and TGF-β signaling in cancer

Authors:

Grant Greene[1], Ian Zonfa[1], Erzsébet Ravasz Regan[1]*

Affiliations:

[1] Biochemistry and Molecular Biology, College of Wooster, Wooster, OH 44691, U.S.A.

* Corresponding Author

Abstract

The tumor microenvironment aids cancer progression by promoting several cancer hallmarks, independent of cancer-related mutations. Biophysical properties of this environment, such as the stiffness of the matrix cells adhere to and local cell density, impact proliferation, apoptosis, and the epithelial to mesenchymal transition (EMT). The latter is rate-limiting step for invasion and metastasis, enhanced in hypoxic tumor environments but hindered by soft matrices and/or high cell densities. As these influences are often studied in isolation, the crosstalk between hypoxia, biomechanical signals, and the classic EMT driver TGF-β is not well mapped, limiting our ability to predict and anticipate cancer cell behaviors in changing tumor environments. To address this, we built a Boolean regulatory network model that integrates hypoxic signaling with a mechanosensitive model of EMT, which includes the EMT-promoting crosstalk of mitogens and biomechanical signals, cell cycle control, and apoptosis. Our model reproduces the requirement of Hif-1α for proliferation, the anti-proliferative effects of strong Hif-1α stabilization during hypoxia, hypoxic protection from anoikis, and hypoxia-driven mechanosensitive EMT. We offer experimentally testable predictions about the effect of VHL loss on cancer hallmarks, with or without secondary oncogene activation. Taken together, our model serves as a predictive framework to synthesize the signaling responses associated with tumor progression and metastasis in healthy vs. mutant cells. Our single-cell model is a key step towards more extensive regulatory network models that cover damage-response and senescence,

integrating most cell-autonomous cancer hallmarks into a single model that can, in turn, control the behavior of in silico cells within a tissue model of epithelial homeostasis and carcinoma.

Author Summary

The cellular environment in and around a tumor can aid cancer progression by promoting several cancer hallmarks. This environment can affect growth and cell death, as well as a phenotype change that renders cells migratory and invasive: the epithelial to mesenchymal transition. Hypoxia (low oxygen availability) is known to promote this transition, while the attachment of cells to soft matrices or high cell density environments hinders it. These influences are often studied in isolation. As a result, their crosstalk is poorly understood. To address this, we have built a network model of cellular regulation that integrates a cell's responses to hypoxia, the biophysical environment, and growth signals to model cell division, death, and the epithelial to mesenchymal transition in environments cells encounter during metastatic tumor progression. Our model reproduces a wide range of experimental cell responses and offers experimentally testable predictions about the emergence of cancer hallmarks driven mutations that affect the hypoxic response. Our single-cell model is a key step towards more extensive cell-scale models that also include cell aging and damage response. These, in turn, can serve as building blocks of a larger tissue model of healthy vs. cancerous epithelia.

Introduction

Tumor formation is marked by the development of mutations leading to dysregulated cell growth and death. Accumulation of cancer hallmarks is further aided by the tumor microenvironment (TME) – the biochemical composition, biophysical structure of the tissue, and non-cancer cells residing inside and around a tumor, all of which exert a major influence on the development and progression of cancer (1,2). The TME is both variable and dynamic, with primary and secondary metastatic sites found to have differing environments that further vary by cancer origin (3–5). Interestingly, the TME can contribute to the initial formation of tumors, rather than simply relying on stochastic genetic change as originally believed for carcinogenesis (6). As cancer remains the second leading cause of death globally, understanding the unique conditions that promote metastasis contributing to 70-90% of cancer mortality is paramount to identifying therapeutics to both prevent and treat it (7).

A rate limiting step for metastasis is epithelial to mesenchymal transition (EMT), a process where cells gain mesenchymal characteristics and lose their apical-basal polarity; aiding their migration, tissue invasion, and dissemination to secondary sites (8). Yet, the reverse process (MET) is also crucial for tumor growth at secondary sites (9,10). EMT and MET often do not require mutations to arise; rather they emerge due to the phenotypic plasticity of cancer cells responding to the TME. The stepwise process of EMT is controlled by two central double-negative feedback loops (11,12). The first switch flips when an epithelial cell transitions to a

hybrid E/M state, requiring the activation of SNAI1 by extracellular signals, accompanied by repression of the epithelial microRNA miR-34 (13). In this hybrid E/M state, cells lose their apical-basal polarity, become migratory, yet still maintain adherens junctions with neighbors to facilitate collective migration. To complete full EMT, loss of the second epithelial microRNA, miR-200, must occur in conjunction with high expression of the EMT factor ZEB1 (14). This leads to the loss of E-cadherin and all adherens junctions, prompting a full mesenchymal phenotype. While these two feedback loops are but a small part of the regulatory network driving EMT, their central role is illustrated by the fact that hybrid E/M states were first predicted by a computational model of this circuit (11,12), later confirmed *in vitro* (15–18) and *in vivo* (19–22). A series of computational models of increasing complexity followed, exploring the role of phenotypic stability factors (23,24), the connection between hybrid E/M cells and cancer stemness (18), spatial patterning in tumors (25), and the role of biological noise in EMT (26). Most relevant for this study are models that capture the crosstalk between multiple EMT-driving extracellular signals (27). Among these, the influential large Boolean model by Steinway et al. integrated TGFβ, Wnt, Notch, Hedgehog, and serval growth signaling pathways, predicting and verifying several interventions capable of controlling EMT *in vitro* (28,29).

In addition to well-characterized transforming signals such as TGFβ secreted by nearby cells, EMT is influenced by two key aspects of the TME. First, the concentration of oxygen is known to decrease in response to tumor growth (30). The increased size of solid tumors coupled with poor vascularization and vessel

integrity lead to hypoxia – defined as an oxygen supply of < 40 mmHg or < 6% O_2 (31,32). Tumor cells respond to hypoxic conditions with the secretion Vascular Endothelial Growth Factor (VEGF) to induce angiogenesis and fulfil their oxygen demand (33,34). Yet, blood vessel formation within tumors is highly dysregulated and ineffective at relieving hypoxia (32,35). Acute, moderate hypoxia, in turn, promotes invasion and metastasis – an alternative pathway for tumor cells to resolve the oxygen demand by migrating to oxygen rich tissue. Second, EMT is highly dependent on the biophysical environment. Namely, high cell density hinders EMT (36,37), while the increased matrix stuffiness characteristic of fibrotic tissue promotes it (38,39). Both hypoxia and the biophysical environment were shown to contribute to immuno-, radio- and chemotherapy resistance, furthering cancer mortality (40–44). However, the context-dependent crosstalk of hypoxia and the biophysical environment in driving EMT and MET are not well understood.

The hypoxic response occurs through two mechanisms: a canonical response mediated transcriptionally by Hypoxia Inducible Factor (HIF) proteins, and a non-canonical loss of oxygen-dependent degradation enzyme function, increasing the stability of target proteins (31,45–47). HIF proteins are heterodimeric transcription factors comprised of an oxygen-sensitive Hif-α domain paired with a constitutively stable Hif-β domain. Regulation of the Hif-α subunit occurs through the oxygen-dependent hydroxylation of its proline residues, performed by prolyl hydroxylase domain (PHD) enzymes (**Fig. 1A**) (48). This in turn allows for recognition by E3 ubiquitin ligase Von Hippel Lindau protein (pVHL), leading to rapid Hif-1α degradation (49). Additionally, the Factor Inhibiting HIF (FIH) hydroxylase enzyme

uses O_2 as a substrate for asparagine hydroxylation, inhibiting HIF binding to transcription co-activator p300 and thus blocking its transcriptional activity (50). Most higher eukaryotes have three oxygen-sensitive HIFα isoforms; Hif-1α, Hif-2α, and Hif-3α (51). The first discovered and most well understood subunit is Hif-1α, stabilized in response to acute hypoxic stress (52). In contrast, Hif-2α is preferentially stabilized during long-term hypoxic reprogramming, offering temporal control over HIF regulation (53,54). Finally, Hif-3α forms a negative feedback-loop with Hif-1α to fine-tune long-term hypoxia, while maintaining its own unique transcriptional activity (55,56). In comparison to the ubiquitously expressed Hif-1α, Hif-2α and -3α are more temporal and cell-specific (51,57,58).

Since the discovery of Hif-1α, several hundred genes have been discovered to be differentially expressed under hypoxia as a result of HIF transcription, affecting a wide array of signaling pathways (59–61). Critically, both mesenchymal factors SNAI1 and ZEB1 are transcriptional targets of Hif-1 (62,63). Additionally, several other mesenchymal markers are shared targets Hif-1 and the classical EMT-inducing TGF-β pathway (64,65). Independent of HIF transcriptional regulation, non-canonical hypoxia responses involving the loss of oxygen-dependent PHD hydroxylation and the accumulation of reactive oxygen species (ROS) through the electron transport chain were also shown to promote EMT. For example, PHD/pVHL has been implicated in repressing Transforming Growth Factor-β (TGF-β), contributing to increased TGF-β expression under hypoxia (66). Moreover, ROS accumulation caused by increased glycolysis under hypoxia contributes to Src activation and PHD inhibition, furthering invasion, metastasis, apoptosis resistance,

155 and treatment resistance (67–69). Src tyrosine kinase activity upregulates ERK
156 (70) and is required for loss of cadherin-dependent cell-cell contacts under hypoxia
157 (71).
158
159 Despite the delineation of molecular pathways responsible for canonical and non-
160 canonical hypoxic responses, downstream effects on the cell can appear
161 paradoxical. For example, the Hif-1α-driven Warburg effect is required for
162 proliferative metabolism (72), yet extreme hypoxia can inhibit proliferation (73,74).
163 While metabolic reprogramming under chronic hypoxia aids proliferation (75), acute
164 stabilization of Hif-1α under hypoxia has been shown to prevent proliferation
165 through strong Myc antagonization (74). Similarly, while hypoxia induces apoptosis,
166 hypoxia-driven EMT confers resistance to anoikis (apoptosis triggered by loss of
167 adhesion) (76,77). The pro- and anti-apoptotic effects of hypoxia are suggested to
168 be distinguished by severity and length, governed by two competing cellular
169 compartments: the cytosol vs. mitochondria. On one hand, hypoxia-driven loss of
170 mitochondria membrane potential and decreased ATP production can increase
171 mitochondrial membrane permeability, resulting in cytochrome C release and
172 downstream caspase cleavage under severe hypoxia (78,79). Under moderate
173 hypoxia, localization of Hif-1α to the mitochondria prevents oxidative-stress
174 induced apoptosis through On the other hand, Inhibitor of Apoptotic Protein-2 (IAP-
175 2) expression increases under hypoxia, providing cytosolic prevention of apoptosis
176 independently of Hif-1α activity (80). Loss of HIF function attenuated these
177 behaviors, demonstrating the necessity of the canonical pathway.

These differing outcomes highlight the need to better map the precise combinations of environmental conditions leading to each response. Furthermore, the effect of the biophysical environment on these diverging responses remails largely unexplored.

The tumor microenvironment is heterogenous, both in terms of the spatial distribution of different tumor-associated cells and temporal differences in its molecular composition. Thus is important to understand how the biophysical environment modulates the phenotypic diversity tumor cell populations (81,82). For example, single-cell sequencing experiments have found heterogeneous expression of epithelial and mesenchymal markers emerging from the same tumor site, confirming a broad range of states within the EMT spectrum (22,83,84). As oxygen availability in tumors is also not static, it is important to understand the interplay between these two highly dynamic pathways: the hypoxic response and the induction of EMT in response to the biophysical environment.

The goal of this study is to map the way hypoxia alters these responses in a biophysical milieu-dependent manner. In a previously published Boolean model of mechanosensitive EMT, we reproduced known effects of the biophysical environment on EMT and TGFβ signaling. We predicted that in the absence of TGFβ, the decision between no response, partial EMT, and full EMT in mitogen-stimulated epithelial cells on a stiff ECM is dictated by cell density (85). Here we expanded this model by including key regulators of the canonical and non-canonical hypoxic response, and integrated their effect on growth factor signaling, proliferation, EMT,

and apoptosis. Our model reproduces the requirement of Hif-1α for normal proliferation (86), as well as the anti-proliferative effects of strong Hif-1α stabilization during hypoxia (73,74). Additionally, we capture the molecular mechanism of Hif-1α mediated SNAI1/2 and ZEB1 upregulation (62,87,63) and reproduce hypoxia-driven EMT (63,88); independent of TGF-β (66) but dependent on a stiff ECM (89). Our model also reproduces hypoxic protection from anoikis (76). We offer experimentally testable predictions about the context-dependent effects of TGF-β signaling on hypoxia-mediated EMT, as well as VHL loss on cancer hallmarks with or without secondary oncogene activation. Taken together, we offer a mechanistic, predictive framework to synthesize the signaling responses responsible for hypoxic behaviors associated with tumor progression and metastasis in healthy vs. mutant cells.

Results

Expression of Hif-1α is Required for Proliferation

To model the way hypoxia contributes to EMT and proliferation, we expanded our previous mechanosensitive Boolean network, which includes a detailed cell cycle control circuit driven by growth signaling (MAPK, PI3K/Akt and mTORC) integrated with cell-cell and cell-ECM adhesion, contact inhibition, control of EMT, and apoptosis (85). Here we incorporated a hypoxia module with both canonical and non-canonical response mechanisms (85) (**Fig. 1A;** model in **SM File 1**). This module captures the acute, moderate hypoxic response, focused on Hif-1α and its

224 downstream transcriptional activity (90). In cells, Hif-1α activation and signaling
225 has two functionally distinct regimes, requiring two Boolean nodes to properly
226 capture its effects. Moderate Hif-1α is activated in response to growth factor
227 signaling under normal O_2 conditions to boost glycolysis and proliferative
228 metabolism; we encode this as *Hif1a_basal* = ON. A stronger activation occurs in
229 response to hypoxic conditions or TGF-β signaling, typically in combination with
230 deactivation of Hif-1α inhibitors such as pVHL (modeled as *Hif1a_High* = ON). Next,
231 we included Hif-1α mediated transcription of mesenchymal markers including
232 SNAI1/2, ZEB1, LEF1, β-catenin (and its subsequent nuclear localization / complex
233 formation with Hif-1α) (46,62,63,91). **Fig. 1B** shows the three stable states (fixed-
234 point attractors) of the isolated EMT module, matching the expected activity of EMT
235 regulators in three distinct phenotypic cell states along the EMT spectrum; namely
236 epithelial (top), hybrid E/M (middle) and mesenchymal (bottom). The full network is
237 shown in **Fig. 1C**, while the Boolean rules and detailed biological justification for
238 each of the 165 nodes and 763 links is included in **SM Table 1**.
239
240 **Figure 1. The hypoxic response affects proliferative signaling and EMT. A)**
241 Regulatory module depicting the canonical and non-canonical hypoxic response,
242 along with influences from other signaling pathways and cell states. **B)** Three stable
243 attractors of the isolated EMT regulatory switch (**SM File 2**). *Orange/blue node*
244 *borders:* ON/OFF. **C)** Modular network representation of our extended Boolean
245 model. *Gray:* inputs representing environmental factors; *dark blue:* Adhesion
246 signals; *red: TGFβ* signaling; *green*: Growth Signaling (*lime green*: basal AKT &
247 MAPK, *bright green:* PI3K/AKT oscillations, *mustard*: mTORC1, *dark green: NF-κB,*
248 *GSK3, FoxO1*); *dark red:* Apoptotic Switch*; light blue:* Contact Inhibition; *pink/light*

orange: Migration; *light brown:* Origin of Replication Licensing; *lilac:* Restriction Switch; *purple:* Phase Switch; *dark orange:* cell cycle processes; *yellow:* EMT switch; *teal:* hypoxic response; → : activation; ⊣ : inhibition.

First, we validated our model by comparing its behavior to 150 experimental assays curated from 13 primary literature papers focused on EMT and hypoxia signaling. The 150 assays covered cell behaviors in response to 19 distinct protein or microRNA perturbations (knockdown/ overexpression) and involved 229 unique statistical tests, listed in **SM Table 2**. Our model reproduced 92% (138) of the 150 assays (207 of 229 statistical tests; auto-generated figures in **SM File 4**). Of the 12 failed assays marked in **SM Table 2**, 7 involved experiments that directly contradict others on the list; the others pointed to model limitations detailed in our *Discussion*. Below, we showcase key validation experiments related to hypoxic signaling, along with a series of model predictions.

To test whether the updated model can reproduce the context-dependent influence of Hif-1α activation on proliferation, we used synchronous Boolean update to map the model's attractors in each cellular environment (*Computational Methods IV*). As our starting cell state, we chose a quiescent epithelial phenotype under normoxia, low mitogen exposure sufficient for quiescence, plated at moderate density (e.g., at a monolayer's edge). We then exposed this cell to increasing concentrations of mitogen (**Fig. 2A,** *full time-course:* **SM Fig. 1**). As Hif-1α is a transcriptional inducer of glycolytic genes, we expected a moderate Hif-1α activity increase in spite of the presence of oxygen, required for maintaining the energy demand associated

with proliferation (92–94). Indeed, our model showed intermittent, moderate Hif-1α activation preceding each division (**Fig. 2A**, *arrows*). The average activity of the *Hif1a_basal* node in a population under increasing mitogen exposure went up in tandem with Myc, Cyclin D1 and Cyclin E (**Fig. 2B**), parallelling the increase in cell cycle progression (**Fig. 2C**). Indeed, loss of Hif-1α under normoxia reduced proliferation in our model (**Fig. 2D**), as demonstrated *in vitro* (86). Yet, high levels of Hif-1α of accumulation was also associated with cell cycle arrest due to Myc inhibition (73,74), reproduced by our model by overexpression of the *Hif1a_High* node in strongly mitogen-stimulated cells (**Fig. 2E**). Strong Hif-1α activation blocks the cell cycle via Myc repression, as demonstrated by partial cell cycle rescue in cells with hyper-active Myc (**SM Fig. 2**). In summary, both over and under-expression of Hif-1α severely limit proliferation in our model, as described in the experimental literature.

Figure 2. Hif-1α is required for proliferation under normoxia. A) Dynamics of relevant regulatory molecule expression/activity during exposure of a quiescent cell to increasing mitogen signaling (60 update-steps of 45%, 65%, 85% and 100% high GF; full network dynamics in **SM Fig. 1A**). *X-axis:* update steps annotated by cell cycle phase (G0: quiescence; G1: start of cell cycle entry; S: DNA synthesis; G2: growth phase 2; M: metaphase; A T: anaphase, telophase, cytokinesis); *y-axis*: nodes organized by regulatory module; *yellow/blue*: ON/OFF; *red arrow:* Hif1a_basal node. **B)** Average expression of *Hif1a_basal* (teal), Myc, CyclinD1 and CyclinE (lilac) in the four consecutive time windows with increasing GF_High input (45%, 65%, 85%, 100%) in an ensemble of 10,000 simulations representing individual cells. **C)** Fraction of time cells spend in quiescent (orange) vs. proliferative (*dark red*) states

298 (*left*) and fraction of time a cell's state matched the G0_G1, G2 or SAC state of the
299 phase switch (*right*) in subsequent time windows with increasing growth factor
300 (45%, 65%, 85%, 100%) in an ensemble of 10,000 cells. **D)** Fraction of time cells
301 spend quiescent (*orange*) vs. proliferative (*dark red*) states (*left*) and fraction of time
302 cell states match the G0_G1, G2 or SAC state of the phase switch (*right*) at
303 increasing levels of *Hif1a_basal* knockdown (*autocrine TGF-β:* 5% TGFb_secr
304 knockdown). **E)** Fraction of time cells spend in quiescence (*orange*) vs. in cell cycle
305 (*dark red*, *left*) and fraction of time cell states match the G0_G1, G2 or SAC state of
306 the phase switch (*right*) at increasing levels of *Hif1a_High* hyper-activation (*log2*
307 *scale:* 0, 0.625, 1.25, 2.5, 5, 10, 20, 40 and 80% Hif1a_High = ON; *autocrine TGF-*
308 *β:* 5% TGFb_secr knockdown). *Length of time-window for continuous runs:* 500
309 steps (~24 wild-type cell cycle lengths); *total sampled live cell time:* 100,000 steps;
310 *update*: synchronous; *initial condition for all sampling runs*: epithelial cells in GF:1,
311 CellDensity_High:1, Stiff_ECM:1, Trail:0, Self_Loop:1, TGFb_ext:0, Hypoxia:0;
312 *environment of sampling runs:* saturating growth signals (GF_High:1), moderate
313 density (CellDensity_Low:1).

314

315 ## Hypoxia arrests proliferation and induces EMT

316

317 Having demonstrated the role of Hif-1α expression in proliferation under
318 normoxia, we next assessed the effect of the hypoxic response on proliferation and
319 EMT. As described above, Hif-1α overexpression in the presence of oxygen lead to
320 cell cycle arrest due to Myc repression (**SM Fig. 2**) (74). Hypoxia induced a similar
321 cell cycle arrest in our model, as lack of oxygen blocked PHD2 hydroxylation and

downstream VHL-mediated Hif-1α degradation (**Fig. 3A**). In addition to cell cycle arrest, our simulation showed hypoxia-induced EMT in cycling cells (**Fig. 3A**), as expected from experimental literature (86,89,95) . Namely, hypoxia resulted in Hif-1α mediated transcription of mesenchymal transcription factors SNAI1/2, ZEB1, LEF1, and nuclear β-catenin, generating a mesenchymal phenotype and complete loss of epithelial markers (**SM Fig. 3A**) (63,91,96). In addition, non-canonical (Hif-1α independent) stabilization of IKKβ due to a lack oxygen-dependent hydroxylation by PHD lead to NF-κB activation (**SM Fig. 3A**) (97).

As seen in **Figure 3A**, hypoxia triggers autocrine TGF-β signaling due to a combination of oxygen dependent loss of VHL activity (66), Hif-1α mediated activation of TGF-β converting enzyme furin (98), and critically, secretion of TGF-β induced by EMT transcription factors (46,99). Yet, this effect is a consequence rather than driver of EMT under hypoxia, as TGF-β receptor I knockdown does not block hypoxia-induced EMT – though it slows it in mild hypoxia (**Fig. 3B-C**). That said, lack of TGF-β signaling does weaken cell cycle arrest in the presence of mitogens (**Fig. 3D**). Moreover, hypoxic EMT in VHL independent (**Fig. 3B-C**), as PHD2-mediated hydroxylation and degradation of Hif-1α requires oxygen even in VHL-overexpressing cells (**SM Fig. 3B**) (48,100). In contrast, TGF-β can only stabilize Hif-1α in the absence of VHL (**SM Fig. 3C**) (100). As EMT transcription factors induction occurs independently through either Hif-1α or SMAD2/3/4, the two pathways do not rely on each other to promote EMT (**SM Fig. 3D**).

Figure 3. Hypoxia induces EMT and blocks cell cycle independently of TFG-β signaling. A) Dynamics of regulatory molecule expression in a proliferating cell in response to hypoxia (80 / 40 / 40 update-steps of normoxia/hypoxia/normoxia at 95% saturating mitogen exposure and moderate cell density). *X-axis:* update steps annotated by cell cycle phase (G0: quiescence; G1: start of cell cycle entry; S: DNA synthesis; G2: growth phase 2; M: metaphase; A/T: anaphase, telophase, cytokinesis); *y-axis*: nodes organized by regulatory module; *yellow/blue*: ON/OFF; *black/white labels:* relevant phenotypes; *update*: synchronous. **B-C)** Fraction of time cells at moderate density exposed to weak (B) or strong mitogens (C) spend in epithelial (*yellow*), hybrid E/M (*dark yellow*) and mesenchymal (*mustard*) states at increasing hypoxia exposure. **D)** Fraction of time strong mitogen-exposed cells spend in quiescence (*orange*) vs. in cell cycle (*dark red*) at increasing hypoxia exposure. **B-D)** *1st row:* wild-type; *2nd row*: 100% IKK□/β knockdown; *3nd row*: 100% TGFβ-RI knockdown; *4th row:* 100% pVHL hyper-activation. *log_2 X axis:* 0, 0.625, 01.25, 2.5, 5, 10, 20 and 40 hypoxia; *black dashed line:* 80%; *white stars:* altered from wild-type; *length of time-window for continuous runs:* 100 steps (~5 wild-type cell cycle lengths); *total sampled live cell time:* 100,000 steps; *update*: synchronous; *initial condition for all sampling runs*: epithelial cells in GF:1, CellDensity_Low:1, Stiff_ECM:1, Trail:0, Self_Loop:1, TGFb_ext:0, Hypoxia:0; *environment of sampling runs:* GF_High = 0.25 (B) or GF_High = 0.95 (C) and moderate density (CellDensity_Low:1); *autocrine TGF-β loop:* 5% TGFb_secr knockdown.

366

367 ## The biophysical environment and oxygen availability
368 ## modulate epithelial to mesenchymal transition and its
369 ## reversal

370

371 Experimental literature on the crosstalk between the hypoxic response and
372 ECM primarily focuses on hypoxia induced remodeling by fibroblasts, or induction of
373 the Warburg effect (101–105), leaving the interplay of hypoxia and ECM stiffness or
374 cell density underexplored. One of the few direct studies on the dependence of EMT
375 on ECM stiffness under hypoxia demonstrated that mesenchymal marker induction
376 under hypoxia positively correlate with matrix stiffness in vitro[12]. To test whether
377 our model can reproduce this, we started our next simulation with a quiescent
378 epithelial cell on a soft ECM, at low density and under hypoxia (arrested due to an
379 inability to stretch as well as hypoxia). We then gradually increased ECM stiffness
380 by stochastically turning ON the *Stiff_ECM* node, until its saturation (*Stiff_ECM* =
381 ON). As shown in **Figure 4A**, mesenchymal markers gradually turned on starting
382 from *Stiff_ECM = 0.5*, and cells maintained a fully mesenchymal state by *Stiff_ECM*
383 *= 0.75* (complete time-course: **SM Fig. 4A***)*. In contrast, cells under normoxia
384 underwent partial EMT and entered the cell cycle, never reaching high levels of
385 ZEB1 to repress miR-200c and E-cadherin expression (**Fig. 4B**, **SM Fig. 4B**). The
386 average SNAI1 activity of a heterogeneous population of *in silico* cells at increasing
387 ECM stiffness closely resembled its relative expression *in vitro* (**SM Fig. 5A**).

Additionally, the effect of matrix stiffness on migration was stronger under hypoxia, aligning with the study's wound-healing results (**Fig. 4B**, *middle row*). Lastly, our model predicts that matrix stiffness affects hypoxia-induced EMT more profoundly than TGF-β induced EMT (**SM Fig. 5B**). The EMT-induction threshold of hypoxia is increases rapidly on softer ECMs, while the effect on TGF-β-induced EMT is significantly milder. We further predict that on soft ECMs that cannot support stress fiber formation and migration, only a combination of strong hypoxia and near-saturating TGF-β can induce EMT (**SM Fig. 5B**, *left*). In contrast, high cell density blocks EMT in response to either signal as well as their combination, while isolated mitogen-stimulated cells undergo biomechanically induced EMT even in the absence of hypoxia or external TGF-β (**SM Fig. 5C**) (85).

Figure 4. A stiff ECM aids hypoxia-induced EMT. A) Dynamics of relevant regulatory molecule expression in a quiescent cell on a soft ECM under hypoxia, in response to increasing ECM stiffness (50 update-steps of 0, 25, 50, 75 and 100% Stiff_ECM = ON at saturating mitogen exposure, moderate cell density and 5% TGFb_secr knockdown). *X-axis:* update steps; *y-axis*: nodes organized by regulatory module; *yellow/purple/blue scale*: 100% ON/ 50% on / 100% OFF; *black/white labels:* relevant phenotypes; *update*: synchronous; *full time-course:* SM Fig. 4A. **B)** Fraction of time normoxic (*left*) vs. hypoxic (*right*) cells at moderate density and saturating mitogen exposure, plated on ECM of increasing stiffness, spend in: *top:* epithelial (*yellow*), hybrid E/M (*dark yellow*) and mesenchymal (*mustard*) states; *middle*: non-migrating (*light pink*), slow-migrating (*dark pink*) and fast-migrating (*brow-pink*) states; *bottom:* quiescence (*orange*) vs. in cell cycle (*dark red*). *Length of time-window for continuous runs:* 100 steps (~5 wild-type cell cycle lengths);

total sampled live cell time: 100,000 steps; *update*: synchronous; *initial condition for all sampling runs*: epithelial cells in GF:1, CellDensity_Low:1, Stiff_ECM:1, Trail:0, Self_Loop:1, TGFb_ext:0, Hypoxia:0; *environment of sampling runs:* Hypoxia:0(*left*)/1(*right*), GF_High:1, CellDensity_Low:1; *autocrine TGF-β loop:* 95% (5% TGFb_secr knockdown).

Loss of the Hif-1α repressor VHL aids metastatic cell behaviors

Development of clear cell renal cell carcinoma (ccRCC) is marked by mutations to Von Hippel Lindau gene, resulting in reduced expression or inactive forms of VHL protein and aberrant Hif-1α expression under normoxia as well as hypoxia (106). This mutation contributes to ccRCC being the 13th most common malignancy throughout the world (107), as well as its reduced treatment efficacy and markedly high mortality rate (108). While VHL loss is a hallmark of ccRCC, this mutation alone is unable to consistently induce tumorigenesis in mice (109,110). Modeling VHL deficient cells, we predict that the loss of VHL can drive metastatic cell behaviors under biophysical microenvironments that do not induce EMT in wild-type cells. To this end, we simulated wild type vs. 90% VHL knockdown in cells on soft to stiff ECM, at densities ranging from isolated cells to dense fully confluent monolayers under normoxia (**SM Fig. 6A**, *top left*). In the presence of a near-saturating growth stimulus, only cells with some access spreading space and a very stiff ECM underwent full EMT. In contrast, the combination of ECM and density

436 values leading to EMT were significantly expanded in VHL deficient cells. Loss of
437 VHL boosted full EMT rates particularly at moderate ECM stiffness, and in cells that
438 had only intermittent access to space to establish horizontal polarity (**SM Fig. 6A**,
439 *middle/bottom left*). While hypoxia blunted its effects, the boost to EMT was still
440 significant at moderate hypoxia (**SM Fig. 6A**, *middle/right columns*). As loss of VHL
441 stabilized Hif-1α, it also resulted in a full cell cycle arrest (**SM Fig. 6B**), indicating
442 that a boost to EMT in VHL-null cells would be counterbalanced by arrested growth.
443
444 Overall, our VHL-deficient simulations indicate that a combination of VHL loss
445 and cell cycle-promoting oncogene activation is required for cancer progression,
446 breaking Hif-1α and/or EMT-induced cell cycle arrest. Indeed, ccRCC tumors with a
447 VHL missense mutation often harbor Cdk4/6 and/or Cyclin D amplification and are
448 highly proliferative (111). Moreover, the most proliferative subtype of ccRCC is both
449 VHL deficient and have enhanced MYC activity (112). To test whether our model
450 could reprocure proliferation rescue in VHL-null cells, we re-ran the above
451 simulations at varying ECM stiffness and cell density in VHL-deficient cells with or
452 without Myc and/or Cyclin D hyper-activation (**SM Fig. 7A**). Intriguingly, only joint
453 hyper-activation of Myc and Cyclin D could significantly boost the proliferation of
454 VHL-deficient cells (**SM Fig. 7B***, left*). This co-occurred with a mild reduction in EMT
455 compared to VHL deficiency alone (**SM Fig. 7B***, right*). In contrast, pairing Cyclin D
456 with ccRCC-associated mutations upstream in the PI3K or MAPK pathway, such as
457 PI3K/mTORC1/ERK hyper-activation or p21/PTEN loss (113), only led to weak cell
458 cycle rescue (**SM Fig. 7C**; though most of these combinations also mildly boosted

EMT; not shown). Pairing Myc with the same cancer mutations only yielded weak rescue with p21 loss, no cell cycle otherwise (**SM. Fig. D**).

Hypoxia prevents anoikis and epithelial apoptosis in response to TGF-β

In addition to inducing a mesenchymal state, the lack of oxygen has been shown to block anoikis and apoptosis; further contributing to the mortality rate of hypoxic tumor formation (79,114). As previously shown in Sullivan et al.(85), our mechanosensitive model can reproduce anoikis mediated epithelial cell death in response to detachment from the extracellular matrix. To test if our model could also replicate hypoxia-mediated evasion of anoikis, we simulated detachment of a quiescent, isolated epithelial cell from a soft ECM exposed to saturating growth factors (**Fig. 5A**; *full time-course:* **SM Fig. 8**). In contrast to normoxia, hypoxia repressed pro-apoptotic factor activation and conferred anoikis resistance (76,115). This was due to the ability of cells suspended under hypoxia to maintain high levels of MAPK signaling and basal AKT activity. This was supported by hypoxia- and ROS-mediated Src upregulation, an effect that did not require integrin-mediated attachment and thus prevented anoikis (**Fig. 5A***, right*) (76). The non-canonical hypoxic response also contributed anoikis resistance through NF-κB nuclear translocation, reinforcing BCL-2 and BCL-X_L expression (116,117). Along similar lines, our model reproduces TGF-β induced apoptosis of epithelial cells on a soft matrix (**Fig. 5B***, left*) (118). Specifically, the model depicts an increase in BAX/BIM

482 signaling along with BCL-X_L loss, followed by apoptosis. In comparison, cells
483 exposed to TGF-β in a hypoxic environment are predicted to resist apoptosis
484 through increased Src and MAPK activity (**Fig. 5B**, *right*).
485
486 **Figure 5. Hypoxia confers anoikis resistance and protection from TGF-β**
487 **induced epithelial cell apoptosis on a soft ECM. A)** Dynamics of relevant
488 regulatory molecule expression in a quiescent cell detached from a soft ECM in
489 normoxia (*left*) vs. hypoxia (*right*) (20 update-steps on soft ECM, 50 update-steps
490 detached, 100% high GF). **B)** Dynamics of relevant regulatory molecule expression
491 in a quiescent cell on a soft ECM, exposed to exogenous TGF-β in normoxia (*left*) vs.
492 hypoxia (*right*) (20 update-steps no TGF-β, 50 update-steps 100% TGF-β). *X-axis:*
493 update steps; *y-axis*: nodes organized by regulatory module; *yellow/blue*: ON/OFF;
494 *black/white labels:* relevant phenotypes; *update*: synchronous; *full time-course:* **SM**
495 **Fig. 8**.

496

497 Hypoxia and reoxygenation can drive the metastatic
498 cascade in the absence of exogenous transforming
499 signals

500
501 Next, we aimed to identify the biophysical microenvironments required for MET
502 following reoxygenation, a crucial step in the formation of secondary tumors (119).
503 To simulate a metastatic cascade, allowing for both intravasation and extravasation

504 from a solid tumor, we simulated a sequence of microenvironments designed to
505 mimic the signals metastatic cells experience en route from a solid tumor towards a
506 new metastatic site. To do this, we started with an epithelial cell at high cell density
507 on a stiff ECM, such as the basement membrane (120) (**Fig. 6A**, *pulse 1*). In a
508 growing solid tumor, this cell is likely to experience hypoxia (**Fig. 6A**, *pulse 2*). Yet,
509 due to density-dependent contact inhibition of proliferation as well as migration,
510 this epithelial cell requires the loss of neighbors (e.g., apoptosis of a neighbor) to
511 gain the room required for hypoxia-driven EMT (**Fig. 6A**, *pulse 3*). Migrating away
512 from the solid tumor, the cell can now reach areas of lower density and adequate
513 oxygen, while maintaining its mesenchymal state (**Fig. 6A**, *pulse 4*).
514
515 As hypoxia induces self-sustaining autocrine TGF-β signaling (14), transitioning
516 back to an epithelial state requires breaking the autocrine loop. This can happen
517 due to non-saturating TGF-β secretion in transit through the blood stream, where
518 cells have no access to a stiff ECM to keep mechanosensitive EMT signals active
519 (**Fig. 6A**, *pulse 5*). As a result, upon entering the vasculature, detachment from the
520 ECM and other cells is a crossroad with two phenotypic outcomes: cells that
521 maintain a mesenchymal state avoid anoikis, whereas cells that revert to an
522 epithelial state undergo apoptosis (**Fig. 6A**, *pulse 5*). Surviving cells then transition
523 to an epithelial state upon reaching high cell density in the new tissue (**Fig. 6A**,
524 *pulse 7*). From here, they can re-enter a proliferative hybrid E/M state once they
525 escape contact inhibition (121). This completes the metastatic cascade, leading to
526 new tumor growth. In contrast to cells with non-saturating autocrine TGF-β
527 signaling, saturating TGF-β secretion prevents apoptosis in nearly all cells

528 undergoing the metastatic cascade (**SM Fig. 9**). That said, even slight
529 perturbations of the autocrine loop, modeled by reducing *TGFb*_secr, are predicted
530 to have a major impact on the rate of apoptosis in the bloodstream, as well as upon
531 transitioning onto a soft ECM (**SM Fig. 10**).
532
533 **Figure 6. As cells follow the metastatic cascade, hypoxia-induced EMT**
534 **protects cells in circulation, reversed at the secondary site by high cell**
535 **density. A)** Dynamics of relevant regulatory molecule expression in an ensemble of
536 1000 quiescent epithelial cell exposed to a sequence of microenvironments along the
537 metastatic cascade (100 update-steps per pulse). *Pulse 1:* normoxia, stiff ECM, high
538 density; *Pulse 2:* hypoxia, stiff ECM, high density; *Pulse 3:* hypoxia, stiff ECM,
539 medium density; *Pulse 4* (invasion)*:* normoxia, stiff ECM, very low density; *Pulse 5*
540 (intravasation)*:* normoxia, no ECM, no neighbors; *Pulse 6* (extravasation)*:* normoxia,
541 soft ECM, low density; *Pulse 7* (MET)*:* normoxia, stiff ECM, high density; *X-axis:*
542 update steps; *y-axis*: nodes organized by regulatory module; *yellow/blue*: ON/OFF;
543 *black/white labels:* relevant phenotypes; *update*: synchronous; *autocrine TGF-β:* 5%
544 TGFb_secr knockdown; *full time-course:* **SM Fig. 8**. **B)** Average fraction of time an
545 ensemble of 1000 cells spend in *top:* non-migrating (*light pink*), slow-migrating
546 (*dark pink*) and fast-migrating (*brow-pink*) states; *middle*: epithelial (*yellow*), hybrid
547 E/M (*dark yellow*) and mesenchymal (*mustard*) states; *bottom:* survival (*red*) vs. in
548 apoptotic (*dark red*) states for each pulse along the metastatic cascade in panel A.
549
550 Another way to visualize the environment changes driving EMT and MET is to
551 highlight the cell state sequence the above steps push our model through, shown
552 on a comprehensive map of all relevant stable model phenotypes (attractors)

organized by microenvironment (**SM Figure 11**). Taken together, our mechanosensitive model can reproduce hypoxia-driven EMT, and its reversal based on a realistic sequence of its biophysical environments, depicting molecular signaling which occurs throughout the metastatic cascade.

Discussion

Despite the prevalence of hypoxic tumor microenvironments during solid tumor progression, the combined effect of hypoxia and the biophysical environment on cancer hallmarks remains underexplored. Here, we have built a dynamic regulatory network model focused on depicting the molecular signaling that occurs in response to oxygen deprivation (**Fig. 1**). To do this, we incorporated a hypoxic response module into our previously published mechanosensitive EMT model (85). Unlike published models exploring individual hypoxia-induced phenotypes (122–125), our model captures Hif-1α mediated transcription responsible for i) the induction as well as inhibition of proliferation (**Fig. 2**), ii) propelling EMT in a mechanosensitive manner (**Fig. 3-4**), and iii) preventing cell death in response to a changing TME (**Fig. 5**). Taken together, our model can reproduce cell state changes along a full metastatic cascade (**Fig. 6**), providing insight into the effects of a continuously changing biophysical environment during secondary tumor formation. The resulting cell behaviors cover cell-autonomous aspects of several cancer hallmarks, including *sustaining proliferative signaling*, *evading growth suppressors*, *activating invasion and metastasis*, *resisting cell death*, and *unlocking phenotypic plasticity* (126).

575

576 1. *Sustaining proliferative signaling & evading growth suppressors.* Our model
577 captures the paradoxical relationship between Hif-1α and proliferation. On
578 one hand, Hif-1α is required for proliferation through its role in upregulation
579 of the glycolytic machinery, including GLUT1, LDH-A, ALDA, and more
580 (modeled indirectly; **Fig. 2D**)(127). On the other hand, the increased
581 stability of Hif-1α under hypoxic conditions is known to induce cell cycle
582 arrest through functionally repressing Myc, a key driver of proliferation (**Fig.**
583 **2E**) (73,74). Indeed, our model predicts that Myc hyperactivation can rescue
584 the cell cycle under hypoxia (**SM Fig. 2**). In comparison to the effects of
585 *acute* oxygen deprivation captured by our model, *chronic* hypoxia increases
586 proliferation through Hif-2α-induced Myc transcription, increased MAPK/ERK
587 signaling, and YAP1 activation (128–130). Capturing this temporal shift in our
588 model is an area of future interest.

589

590 2. *Activating invasion and metastasis.* While the effects of hypoxia on EMT are
591 well-documented, the mechanosensitive nature of this response, as well as
592 its crosstalk with TGF-β signaling, have not been modeled individually or
593 collectively. Our model shows that hypoxia can induce EMT in cycling cells
594 (**Fig. 3**) (86), as long as they have access to a stiff ECM and some space to
595 spread (**Fig. 4**, **SM Fig 5**) (89). In contrast, normoxic cells only undergo
596 hybrid E/M in all but the most EMT-promoting biophysical environments (**SM**
597 **Fig. 5**). Once established, a mesenchymal state is maintained regardless of
598 hypoxia due to its ability to induce autocrine TGF-β signaling (**Fig. 3A**), even

599 in the presence of hyper-active VHL (100). Yet, this autocrine signal is not
600 required for EMT in hypoxic cells, as loss of TGF-β Receptor I does not block
601 the transition (**Fig. 3B**) (100). In contrast, TGF-β can only boost Hif-1α
602 stabilization in VHL-deficient cells. These nuances of crosstalk highlight the
603 importance of modeling the biophysical environments and genetic
604 interactions that compound the loss of VHL, a tumor suppressor pivotal to
605 clear cell renal cell carcinoma (ccRCC) tumorigenesis (108). These cancers
606 have among the highest rates of metastasis and mortality (131). Our model
607 predicts that VHL loss alone, known to predispose patients to cancer (132),
608 can push cells at moderate density and/or on a softer ECM into full EMT.
609 These cells undergo EMT instead of maintaining an epithelial state or a
610 reversible hybrid E/M phenotype required for repairing epithelial damage, as
611 expected in healthy cells (**SM Fig. 6**) (133). Furthermore, we highlight the
612 importance of secondary driver mutations that directly impact cell cycle
613 entry, such as joint cyclin D and Myc amplification / hyperactivation
614 (111,112). These mutations overcome the cell cycle arrest mediated by
615 hyperactive Hif-1α and/or autocrine TGF-β signaling (**SM Fig. 7**), helping
616 cancer cells combine sustained proliferation with an invasive mesenchymal
617 state.
618
619 *3.* *Resisting cell death.* Our model not only reproduces anoikis resistance of
620 epithelial cells under hypoxia (76), but also predicts that hypoxia can protect
621 epithelial cells on a soft ECM from TGF-β-induced apoptosis (**Fig. 5**).
622

4. *Unlocking phenotypic plasticity.* Our simulation of the metastatic cascade, from hypoxia-induced EMT in a primary tumor through anoikis resistance in the bloodstream to cell density-induced MET at a secondary site, our model captures the non-genetic phenotypic plasticity cancer cells tap into as they navigate different combinations of chemical and biomechanical environments (**Fig. 6**). Interestingly, our model predicts that the ability to reach and sustain a fully mesenchymal state, with no break in autocrine TGF-β signaling, serves as an environmental bottleneck for circulating tumor cells (**SM Fig. 9,10**). Moreover, intermittent (non-saturating) TGF-β signaling can also render the transition back onto a soft ECM dangerous, as a weaker mesenchymal program is less apt at warding off the apoptotic effects TGF-β has on epithelial cells on soft ECM (85).

A particular strength of our model is its ability to reproduce a wide array of experimental results in wild type, as well as mutant cells. Namely, the model matched the direction and significance of molecular or phenotypic changed in 138 of 150 independently conduced experimental assays from 13 primary papers focused on hypoxia and EMT (**SM Table 2**), and 7 of its 12 failures were due to contradictory experiments included in our list. This validation lends weight to our predictions, summarized below:

a) We predict that the loss of TGF-β signaling can weaken hypoxia-mediated cell cycle arrest (**Fig. 3D**), and slow down hypoxia-induced EMT in cells with weak mitogenic signaling (**SM Fig. 3**).

b) We predict that soft ECMs drastically raise the hypoxia threshold of EMT, while they impact TGF-β more mildly. On very soft ECMs unable to support stress fiber formation and migration, only a combination of strong hypoxia and near-saturating TGF-β can induce EMT (**SM Fig. 5B**).

c) We predict that breaking the cell cycle inhibitory effects of VHL loss requires combined hyper-activation of Myc *and* Cyclin D (**SM. Fig. 7**; less potent 2-gene combinations involve either p21 loss or Cyclin D hyper-activation). In contrast, upstream mutations that boost PI3K or MAPK signaling (alone or in combination with Myc) cannot overcome cell cycle arrest mediated by Hif-1α and/or TGF-β.

d) We predict that epithelial cells on a soft ECM exposed to TGF-β are protected from apoptosis under hypoxic conditions (**Fig. 5B**).

e) Finally, we predict that circulating mesenchymal cells are highly sensitive to intermittent weakening of autocrine TGF-β signaling, and thus only a fraction of them survives anoikis (**SM. Fig. 9,10**). This could be tested with cell suspension experiments on cells that first undergo EMT, treated with increasing doses of TGF-β or TGF-β RI inhibitors.

Our use of a Boolean modeling framework, despite its advantages in allowing us to build a 165-node regulatory network with 763 links, presents two technical limitations of particular interest here (also discussed in (85)). *First,* modeling autocrine signaling in a Boolean framework means that a positive feedback loop can lock in between a signaling pathway and the transcription/secretion of the signal itself, such as TGF-β. This loop implicitly assumes that a single mesenchymal cell

produces sufficient levels of bio-available TGF-β to maintain saturating signaling on its own receptors; an assumption that is likely problematic. To get around the resulting artifacts, we intentionally disrupted autocrine signaling using a 5% reduction in secreted TGF-β in most of our simulations. This confers some reversibility to EMT, permitting a fluid coexistence of mesenchymal and hybrid E/M cells, the latter of which can divide. Yet, it is possible that *in vitro* the slow division of mostly mesenchymal cells is not due to temporary loss of TGF-β signaling (as modeled), but to the fact that even saturating levels of TGF-β do not fully block cell cycle entry in mesenchymal cells.

A second technical limitation, detailed in (85), relates to our Boolean approximation of ECM stiffness and cell density. There are three qualitatively distinct regimes for these inputs: no ECM / soft ECM not capable of supporting stress fibers and growth / stiff ECM that does. Similarly for density: no neighbors capable of making junctions / some neighbors but also some space / full confluency with no room to expand. Our Boolean model uses two linked nodes for each input, generating a 0 / low / high state. This setup results in distinct signals in the 0 to low vs. the low to high regimes, without overlap between them. This could result in more rigid model responses near these boundaries than expected *in vitro.*

A different class of model limitations relates to the signaling biology we choose to include or ignore. *First,* the five experiments our models failed to match that did not contradict other data highlighted that at present our model is missing the molecular mechanism responsible for Hif-1α-mediated G2 arrest (our model only

694 arrests in G1), as well as hypoxia-induced apoptosis (not modeled by choice).
695 *Second*, we restricted our focus to the *acute* hypoxic response governed primarily
696 by Hif-1α stabilization. Chronic hypoxia leads to a different set of responses our
697 model does not cover, as they are induced by Hif-2α stabilization (134). Despite
698 some conflicting data, it is generally accepted that the third HIF subunit, Hif-3α,
699 prevents Hif-1α transcriptional activity through sequestration of Hif-1β in a cell-type
700 specific manner (135,136). Expansion of the model to include these Hif-α subunits
701 are promising future directions required for modeling the temporal control of cell
702 fates under hypoxia.
703
704 *Third,* Hif-1α is a metabolic regulator, yet we only included its effects on energy
705 metabolism indirectly. The inclusion of a nutrient stimulus such as glucose, and the
706 energy sensing pathways that intersect with cell cycle entry modeled, in part, in
707 (137) would allow for a more precise accounting of the hypoxic response. For
708 example, apoptosis is differentially regulated based on nutrient loss in the presence
709 or absence of Hif-1α, as Hif-1α prevents metabolic stress-induced apoptosis (94).
710 Glucose transporters GLUT1/3 are also upregulated in mesenchymal cells,
711 demonstrating a shift towards glycolysis during EMT and suggesting a dependence
712 of EMT on nutrient levels for under hypoxia and/or normoxia (138). A future
713 expansion of our model could cover these responses, further mapping the
714 environment-combinations most conducive to EMT and MET.
715
716 *Fourth,* our model excludes several signaling pathways known to be differentially
717 regulated under hypoxia, such as Wnt, Sonic Hedgehog (Shh), Notch, Interleukin-6,

or TNF-α (139–146). Thus, we operate under the implicit assumption that these signals are induced at equal levels in response to all stimuli tested within our model – even though it is their regulation may also be mechanosensitive. These signals are also implicated in mediating EMT, preventing apoptosis, and contributing to the spatial and temporal regulation of EMT in response to a changing TME (147). Overall, the integration of these pathways may offer further contextual insight into cancer-associated behaviors increased by hypoxic tumor microenvironments.

Our model's replication of the metastatic cascade is a simplification of the highly complex tumor and blood microenvironments experienced by circulating tumor cells. Of note, extensive research has yielded both increasing and decreasing metastatic potential through interactions with neutrophils, cancer associated fibroblasts (CAFs), macrophages, platelets, and other cell types, all of which are missing from our single-cell modeling approach (148–151). As an example, interactions with platelets can upregulate TGF-β signaling and EMT, which help prevent cell death during the circulating phase (152).

The model boundaries highlighted above stem, in part, from our single cell approach. We find this single cell focus valuable for mapping the rules that govern cell behavior in different microenvironments, a critical step towards building multiscale models of cell communities and tissue architectures needed to approach the complexity of tumor formation, tumor evolution and metastatic disease. Long-term, our goal is two-fold. On the *single cell* modeling side, we plan to integrate the model from this study with our Boolean model of mitochondrial dysfunction-

associated senescence, which shares this model's growth signaling / cell cycle and apoptosis modules (137). We will follow this with a detailed model of damage-induced cell cycle arrest mechanisms and a model of deep senescence, which can reverse mitochondrial dysfunction (153), but it is at least partially blocked in cells that underwent EMT (154,155). The resulting single-cell model would be able to address most cell-autonomous cancer hallmarks. On the *tissue* modeling side, the above single-cell model can serve as the engine inside agents of multicellular, spatial model of epithelial homeostasis and carcinoma development.

Computational Methods

I. Boolean model building. To build our model we extended our previously published mechanosensitive EMT model (85) with a hypoxia-sensing signaling module. The model synthesizes experimental data from 540 papers into a 165-node Boolean network with 763 regulatory links. All links and regulatory functions are experimentally justified in **SM Table 1**. Our model construction approach, the rationale for using synchronous update, storing our model in *Dynamically Modular Model Specification* (*.dmms*) format are detailed in the *Supplementary Methods* of (137) and STAR Methods of (85). All model files and other files required to run the model and reproduce all results, are packaged into **SM Files 1-3**.

II. Model availability. Model files in *SBML* format (used by BioModels (156), *GinSim* (157) and *The Cell Collective* (158)), *dmms* format (used by our discrete-state modeling software *dynmod*), *BooleanNet* format (used by the BooleanNet

764 Python library (159)), and an editable network visualization in *graphml* format
765 (read by yED (160)) are included in **SM Files 1**.

766 ***III.* Dynmod *Boolean modeling software.*** Boolean simulations and analysis
767 were performed with the discrete-state modeling software *dynmod* (137), available
768 on GitHub at *https://github.com/Ravasz-Regan-Group/dynmod* (our justification for
769 using in-house software, along with instructions to install Haskell and compile
770 *dynmod* are detailed in the *Suppl. Methods* of (137)). Briefly, our code can: **a)**
771 automatically map each attractor to a combinatorial phenotype profile (e.g.,
772 quiescent, alive, MiDAS) based on user-defined signatures attached to regulatory
773 switches; **b)** visualize and filter attractors of interest via their phenotype profiles,
774 organizing them within a coordinate system of independent environmental input-
775 combinations; **c)** set up simulations by specifying the initial environment and
776 phenotypic state of the cell, rather than each node state; **d)** collect phenotype
777 statistics on large ensembles of non-interacting cells (independent simulation runs)
778 in non-saturating environments and/or non-saturating perturbations (e.g., 10%
779 Hypoxia, 50% VHL inhibition); **e)** generate simulation-series that explore the
780 model's behavior across a range of environmental inputs, combinations of 2-3
781 inputs, and/or the effects of increasing node knockdown / hyper-activation (alone
782 or in combination with changing environmental input levels; with/without additional
783 background mutations); and **f)** use metadata from *dmms* files to generate a
784 formatted table with all biological documentation (**SM Table 1**).
785

786 To run simulations (including attractor sampling), *dynmod* parses user-generated
787 experiment files (*.vex* format). The **SM File 1** package includes two *.vex* our

readers can use to reproduce all simulations used in our figures (*Hypoxia_EMT_Main_Fig.vex, Hypoxia_EMT_SM_Fig.vex*). Similarly, the **SM File 2** package contains the isolated EMT module model (*EMT_Module_Hypoxia.dmms*), the *EMT_Module.vex* file, and time courses that showcase the model attractors visualized on **Fig. 1B**. Finally, **SM File 3** contains the *.vex* file and script required for rerunning our validation experiments (see below). Additional information to run the simulations is available upon request from E.R.R.

***IV. Attractor detection with* dynmod.** *Dynmod* uses synchronous update to find stable phenotypes and/or oscillations (attractors) via a stochastic sampling procedure (161) detailed in (162–164,85). Briefly, we typically find attractors by running noisy time-courses of length $T=25$ with noise $p=0.02$ from $N=100$ different random initial conditions for each unique combination of environmental inputs ($N_{total} = 100*2^7 = 128{,}000$ random initial conditions). For each observed state along these time-courses, the synchronous attractor basin is determined, recorded, and exported as a *.csv* file (*Greene_Hypoxia_Model_attractors_a100_25_2.0e-2.csv* in the **SM File 1** package). To re-sample the model's attractors, edit the *Sampling*{…} command block near the top of *Hypoxia_EMT_Main_Fig.vex* to switch from the currently active *Read:* directive to the commented-out *Sample:* line.

***V. Running simulations with* dynmod.** Precise use of each command is described in *Hypoxia_EMT_Main_Fig.vex* and *Hypoxia_EMT_SM_Fig.vex* (in **SM File 1**), which are executed by *dynmod* using the **-e** command-line tag:

```
dynmod Hypoxia_EMT_Model.dmms -e Hypoxia_EMT_Main_Fig.vex
dynmod Hypoxia_EMT_Model.dmms -e Hypoxia_EMT_SM_Fig.vex
```

These files include instructions to simulate and visualize: **a)** synchronous time courses from a subset of cell states in a given initial environment, exposed to reversible changes in a single environmental signal (e.g., **Fig. 2A**); **b)** non-saturating environments where an input is stochastically tuned between 0 and 1 (e.g., **Fig. 4A**); **c)** partial or full knockdown/hyper-activation of arbitrary sets of nodes (e.g., **Fig. 3**; justification and limitations in (85)); **d)** combine these in an arbitrary sequence of perturbations and environments defined in distinct time windows (e.g., **Fig. 6**); **e)** average activity of all nodes and/or all module phenotypes in an ensemble of independent cells (e.g., **Fig. 2B**); **f)** bar charts of the activity of user-specified nodes and/or module phenotypes, averaged over an ensemble of independent runs and across each distinct time window of an experiment (e.g., **SM Fig. 3**); **g)** bar charts and heatmaps showing the model's behavior (module phenotype states) across a range of environments and/or node perturbations (e.g., **SM Fig. 6**).

VI. Model validation. To test the model's ability to reproduce experimentally observed cell behaviors and/or molecular changes related to EMT in general and hypoxic responses on particular, we curated a list of 150 distinct observations from 13 relevant primary articles (**SM Table 2**). These observations cover knockdown or overexpression of 19 different proteins or microRNAs. For each *in vitro* experiment, we created matching *in silico* experiments or experiment-pairs that mimicked the extracellular environment and perturbations such as knockdowns or overexpression. This extensive validation protocol is included in *Hypoxia_EMT_Validation.vex* (in **SM File 3**). Running

```
dynmod Hypoxia_EMT_Model.dmms -e Hypoxia_EMT_ Validation.vex
```

generates simulation data on a population of cells for each experimental condition. To automate the 229 comparisons, each *in vitro* observation in **SM Table 2** is accompanied by information about the name and location of its matching *in silico* data (experiment names, relevant time windows, code pointing to the correct attractor file). The Python script *Hypoxia Model Validation Script.py* reads a *.csv* version of **SM Table 2**, as well as the simulation data, to perform unpaired t-tests, list, save and summarize the validation results as the percentage of observations our model can reproduce (script and *.csv* in **SM File 3**). Simulation results are considered a match for the experiment if either of the following conditions are met: *i)* there is a significant change in the same direction as the *in vitro* result, and the change is at least 5% of the average of the two values compared, or *ii)* no change, no significant change, or smaller than 5% difference, matching an *in vitro* result showing no significant change. The script also generates figures for each comparison (**SM File 4**); the 17 failed comparisons identified by the script were manually marked with red/orange "*Mismatch*" labels (*red*: model does not match biological outcome; *orange*: different experiments give conflicting results; model matches other outcome).

VII. Metadata table, 2D network visualization and model conversion.

a) To generate a formatted table with all model metadata included in the `.dmms` file, run `dynmod Hypoxia_EMT_Model.dmms -w -s`

This generates a text file with metadata warning (e.g., missing descriptions, citations, unrecognized node/link types), and a folder containing the LaTeX and BibTeX reference files used to render **SM Table 1**. To generate the pdf, use LaTeX or *https://www.overleaf.com*.

b) To generate a `.gml` file read by the network visualization software yED run

```
dynmod Hypoxia_EMT_Model.dmms -g
```

The resulting visualization can be modified in yED to alter node coordinates and node colors. As long as none of the links or groupings are altered in the editing process, and the changes are saved in `.gml` format, running

```
dynmod Hypoxia_EMT_Model.dmms -u Hypoxia_EMT_Model.gml
```

will read the altered coordinates and colors, then generate an updated `.dmms` file (with a new name). **Fig. 1** was generated in yED by manual post-professing of the auto generated `.gml` file (i.e., removal of groups, altered label colors for better contrast, creation of sub-networks).

c) To generate a `.BooleanNet` version of the model, run

```
dynmod Hypoxia_EMT_Model.dmms -t
```

d) To generate the `.sbml` version, use *bioLQM* (http://colomoto.org/biolqm/) with the command:

```
java -jar bioLQM-0.8-SNAPSHOT.jar Hypoxia_EMT_Model_Fine.booleannet
Hypoxia_EMT_Model.sbml
```

VIII. Previously introduced regulatory modules. Detailed descriptions of *Growth factor signaling*, *Replication origin licensing*, *Restriction switch*, *Mitotic*

phase switch, *Apoptotic switch*, *Cell cycle processes, Adhesion, Contact Inhibition, EMT* and *TGF-β signaling* are detailed in (85).

Acknowledgments

We thank Peter L. Regan for the ongoing improvement of the *dynmod* software package used to generate all modeling results. All funding for this study was provided by The College of Wooster. E.R. would like to thank the Henry Luce III Fund for Distinguished Scholarship, the Faculty Development Funds and the Life Sciences Endowed Funds for research support. I.Z thanks the Henry J. Copeland Independent Study Fund for research travel support. G.G. thanks the Biochemistry and Molecular Biology Program for support to present his work.

Author Contributions

G.G. - conceptualization, data curation, formal analysis, investigation, validation, visualization, writing - original draft, writing – review & editing (built hypoxia signaling modules, Boolean model development, ran simulations, designed validation, generated predictions, figures, wrote first draft of the manuscript).

I.Z. - conceptualization, data curation, formal analysis, investigation (built hypoxia signaling modules, Boolean model development, ran simulations).

E.R.R - conceptualization, data curation, formal analysis, funding acquisition, investigation, methodology, project administration, supervision, validation, visualization, writing - original draft, writing – review & editing (supervised project, built hypoxia signaling modules, guided Boolean modeling software development, developed simulation methods, ran simulations, designed validation, generated predictions, figures, edited and finalized manuscript).

References

1. de Visser KE, Joyce JA. The evolving tumor microenvironment: From cancer initiation to metastatic outgrowth. Cancer Cell. 2023 Mar 13;41(3):374–403.

2. Anderson NM, Simon MC. The tumor microenvironment. Current Biology. 2020 Aug 17;30(16):R921–5.

3. Cacho-Díaz B, García-Botello DR, Wegman-Ostrosky T, Reyes-Soto G, Ortiz-Sánchez E, Herrera-Montalvo LA. Tumor microenvironment differences between primary tumor and brain metastases. J Transl Med. 2020 Jan 3;18(1):1.

4. Zeppellini A, Galimberti S, Leone BE, Pacifico C, Riva F, Cicchiello F, et al. Comparison of tumor microenvironment in primary and paired metastatic ER+/HER2- breast cancers: results of a pilot study. BMC Cancer. 2021 Mar 10;21(1):260.

5. Kim R, Keam B, Kim S, Kim M, Kim SH, Kim JW, et al. Differences in tumor microenvironments between primary lung tumors and brain metastases in lung cancer patients: therapeutic implications for immune checkpoint inhibitors. BMC Cancer. 2019 Jan 7;19(1):19.

6. Neophytou CM, Panagi M, Stylianopoulos T, Papageorgis P. The Role of Tumor Microenvironment in Cancer Metastasis: Molecular Mechanisms and Therapeutic Opportunities. Cancers (Basel). 2021 Apr 23;13(9):2053.

7. Dillekås H, Rogers MS, Straume O. Are 90% of deaths from cancer caused by metastases? Cancer Med. 2019 Aug 8;8(12):5574–6.

8. Son H, Moon A. Epithelial-mesenchymal Transition and Cell Invasion. Toxicol Res. 2010 Dec;26(4):245–52.

9. Dongre A, Weinberg RA. New insights into the mechanisms of epithelial–mesenchymal transition and implications for cancer. Nat Rev Mol Cell Biol. 2019 Feb;20(2):69–84.

10. Dudás J, Ladányi A, Ingruber J, Steinbichler TB, Riechelmann H. Epithelial to Mesenchymal Transition: A Mechanism that Fuels Cancer Radio/Chemoresistance. Cells. 2020 Feb 12;9(2):428.

11. Lu M, Jolly MK, Levine H, Onuchic JN, Ben-Jacob E. MicroRNA-based regulation of epithelial–hybrid–mesenchymal fate determination. Proc Natl Acad Sci USA. 2013 Nov 5;110(45):18144–9.

12. Tian XJ, Zhang H, Xing J. Coupled Reversible and Irreversible Bistable Switches Underlying TGFβ-induced Epithelial to Mesenchymal Transition. Biophysical Journal. 2013 Aug;105(4):1079–89.

13. Siemens H, Jackstadt R, Hünten S, Kaller M, Menssen A, Götz U, et al. miR-34 and SNAIL form a double-negative feedback loop to regulate epithelial-mesenchymal transitions. Cell Cycle. 2011 Dec 15;10(24):4256–71.

14. Gregory PA, Bracken CP, Smith E, Bert AG, Wright JA, Roslan S, et al. An autocrine TGF-beta/ZEB/miR-200 signaling network regulates establishment and maintenance of epithelial-mesenchymal transition. Mol Biol Cell. 2011 May 15;22(10):1686–98.

15. Zhang J, Tian XJ, Zhang H, Teng Y, Li R, Bai F, et al. TGF-β-induced epithelial-to-mesenchymal transition proceeds through stepwise activation of multiple feedback loops. Science Signaling. 2014 Sep;7(345):ra91.

16. Grosse-Wilde A, Fouquier d'Hérouël A, McIntosh E, Ertaylan G, Skupin A, Kuestner RE, et al. Stemness of the hybrid Epithelial/Mesenchymal State in Breast Cancer and Its Association with Poor Survival. PLoS One. 2015;10(5):e0126522.

17. Huang RYJ, Wong MK, Tan TZ, Kuay KT, Ng AHC, Chung VY, et al. An EMT spectrum defines an anoikis-resistant and spheroidogenic intermediate mesenchymal state that is sensitive to e-cadherin restoration by a src-kinase inhibitor, saracatinib (AZD0530). Cell Death Dis. 2013 Nov 7;4:e915.

18. Jolly MK, Tripathi SC, Jia D, Mooney SM, Celiktas M, Hanash SM, et al. Stability of the hybrid epithelial/mesenchymal phenotype. Oncotarget. 2016 Mar 17;7(19):27067–84.

19. Dong J, Hu Y, Fan X, Wu X, Mao Y, Hu B, et al. Single-cell RNA-seq analysis unveils a prevalent epithelial/mesenchymal hybrid state during mouse organogenesis. Genome Biol. 2018 Mar 14;19(1):31.

20. Gonzalez VD, Samusik N, Chen TJ, Savig ES, Aghaeepour N, Quigley DA, et al. Commonly Occurring Cell Subsets in High-Grade Serous Ovarian Tumors

Identified by Single-Cell Mass Cytometry. Cell Rep. 2018 Feb 13;22(7):1875–88.

21. Karacosta LG, Anchang B, Ignatiadis N, Kimmey SC, Benson JA, Shrager JB, et al. Mapping lung cancer epithelial-mesenchymal transition states and trajectories with single-cell resolution. Nat Commun. 2019 Dec 6;10(1):5587.

22. Puram SV, Tirosh I, Parikh AS, Patel AP, Yizhak K, Gillespie S, et al. Single-cell transcriptomic analysis of primary and metastatic tumor ecosystems in head and neck cancer. Cell. 2017 Dec 14;171(7):1611-1624.e24.

23. Biswas K, Jolly MK, Ghosh A. Stability and mean residence times for hybrid epithelial/mesenchymal phenotype. Phys Biol. 2019 Jan 29;16(2):025003.

24. Hong T, Watanabe K, Ta CH, Villarreal-Ponce A, Nie Q, Dai X. An Ovol2-Zeb1 Mutual Inhibitory Circuit Governs Bidirectional and Multi-step Transition between Epithelial and Mesenchymal States. PLoS Comput Biol. 2015 Nov 10;11(11):e1004569.

25. Bocci F, Gearhart-Serna L, Boareto M, Ribeiro M, Ben-Jacob E, Devi GR, et al. Toward understanding cancer stem cell heterogeneity in the tumor microenvironment. Proc Natl Acad Sci U S A. 2019 Jan 2;116(1):148–57.

26. Tripathi S, Chakraborty P, Levine H, Jolly MK. A mechanism for epithelial-mesenchymal heterogeneity in a population of cancer cells. PLoS Comput Biol. 2020 Feb;16(2):e1007619.

27. Steinway SN, Zañudo JGT, Ding W, Rountree CB, Feith DJ, Loughran TP, et al. Network modeling of TGFβ signaling in hepatocellular carcinoma epithelial-to-mesenchymal transition reveals joint sonic hedgehog and Wnt pathway activation. Cancer Research. 2014 Nov;74(21):5963–77.

28. Gómez Tejeda Zañudo J, Guinn MT, Farquhar K, Szenk M, Steinway SN, Balázsi G, et al. Towards control of cellular decision-making networks in the epithelial-to-mesenchymal transition. Phys Biol. 2019 07;16(3):031002.

29. Steinway SN, Zañudo JGT, Michel PJ, Feith DJ, Loughran TP, Albert R. Combinatorial interventions inhibit TGFβ-driven epithelial-to-mesenchymal transition and support hybrid cellular phenotypes. NPJ systems biology and applications. 2015;1:15014.

30. Li Y, Zhao L, Li XF. Hypoxia and the Tumor Microenvironment. Technol Cancer Res Treat. 2021 Aug 5;20:15330338211036304.

31. Jiang BH, Semenza GL, Bauer C, Marti HH. Hypoxia-inducible factor 1 levels vary exponentially over a physiologically relevant range of O2 tension. American Journal of Physiology-Cell Physiology. 1996 Oct;271(4):C1172–80.

1001 32. Krock BL, Skuli N, Simon MC. Hypoxia-Induced Angiogenesis. Genes Cancer.
1002 2011 Dec;2(12):1117–33.

1003 33. Saxena K, Jolly MK, Balamurugan K. Hypoxia, partial EMT and collective
1004 migration: Emerging culprits in metastasis. Transl Oncol. 2020 Aug
1005 8;13(11):100845.

1006 34. Jeltsch M, Leppänen VM, Saharinen P, Alitalo K. Receptor Tyrosine Kinase-
1007 Mediated Angiogenesis. Cold Spring Harb Perspect Biol. 2013
1008 Sep;5(9):a009183.

1009 35. Jiang X, Wang J, Deng X, Xiong F, Zhang S, Gong Z, et al. The role of
1010 microenvironment in tumor angiogenesis. Journal of Experimental & Clinical
1011 Cancer Research. 2020 Sep 30;39(1):204.

1012 36. Cichon MA, Nelson CM, Radisky DC. Regulation of Epithelial-Mesenchymal
1013 Transition in Breast Cancer Cells by Cell Contact and Adhesion. Cancer Inform.
1014 2015 Feb 9;14(Suppl 3):1–13.

1015 37. O'Connor JW, Mistry K, Detweiler D, Wang C, Gomez EW. Cell-cell contact and
1016 matrix adhesion promote αSMA expression during TGFβ1-induced epithelial-
1017 myofibroblast transition via Notch and MRTF-A. Sci Rep. 2016 May
1018 19;6(1):26226.

1019 38. Rice AJ, Cortes E, Lachowski D, Cheung BCH, Karim SA, Morton JP, et al. Matrix
1020 stiffness induces epithelial-mesenchymal transition and promotes
1021 chemoresistance in pancreatic cancer cells. Oncogenesis. 2017 Jul
1022 3;6(7):e352.

1023 39. Tian H, Shi H, Yu J, Ge S, Ruan J. Biophysics Role and Biomimetic Culture
1024 Systems of ECM Stiffness in Cancer EMT. Glob Chall. 2022 Mar
1025 20;6(6):2100094.

1026 40. Aldea M, Andre F, Marabelle A, Dogan S, Barlesi F, Soria JC. Overcoming
1027 Resistance to Tumor-Targeted and Immune-Targeted Therapies. Cancer
1028 Discovery. 2021 Apr 1;11(4):874–99.

1029 41. Taeb S, Ashrafizadeh M, Zarrabi A, Rezapoor S, Musa AE, Farhood B, et al. Role
1030 of Tumor Microenvironment in Cancer Stem Cells Resistance to Radiotherapy.
1031 Current Cancer Drug Targets. 2022 Jan 1;22(1):18–30.

1032 42. Zhao D, Mo Y, Neganova ME, Aleksandrova Y, Tse E, Chubarev VN, et al. Dual
1033 effects of radiotherapy on tumor microenvironment and its contribution
1034 towards the development of resistance to immunotherapy in gastrointestinal
1035 and thoracic cancers. Front Cell Dev Biol. 2023 Oct 3;11:1266537.

1036 43. Luqmani YA. Mechanisms of Drug Resistance in Cancer Chemotherapy. Medical
1037 Principles and Practice. 2008 Jul 9;14(Suppl. 1):35–48.

1038 44. Fletcher NM, Belotte J, Saed MG, Memaj I, Diamond MP, Morris RT, et al.
1039 Specific point mutations in key redox enzymes are associated with
1040 chemoresistance in epithelial ovarian cancer. Free Radic Biol Med. 2017
1041 Jan;102:122–32.

1042 45. Appelhoff RJ, Tian YM, Raval RR, Turley H, Harris AL, Pugh CW, et al.
1043 Differential Function of the Prolyl Hydroxylases PHD1, PHD2, and PHD3 in the
1044 Regulation of Hypoxia-inducible Factor *. Journal of Biological Chemistry. 2004
1045 Sep 10;279(37):38458–65.

1046 46. Peng J, Wang X, Ran L, Song J, Luo R, Wang Y. Hypoxia-Inducible Factor 1α
1047 Regulates the Transforming Growth Factor β1/SMAD Family Member 3 Pathway
1048 to Promote Breast Cancer Progression. J Breast Cancer. 2018 Sep;21(3):259–
1049 66.

1050 47. Ananth S, Knebelmann B, Grüning W, Dhanabal M, Walz G, Stillman IE, et al.
1051 Transforming growth factor beta1 is a target for the von Hippel-Lindau tumor
1052 suppressor and a critical growth factor for clear cell renal carcinoma. Cancer
1053 Res. 1999 May 1;59(9):2210–6.

1054 48. Fong GH, Takeda K. Role and regulation of prolyl hydroxylase domain proteins.
1055 Cell Death Differ. 2008 Apr;15(4):635–41.

1056 49. Kamura T, Sato S, Iwai K, Czyzyk-Krzeska M, Conaway RC, Conaway JW.
1057 Activation of HIF1α ubiquitination by a reconstituted von Hippel-Lindau (VHL)
1058 tumor suppressor complex. Proc Natl Acad Sci U S A. 2000 Sep
1059 12;97(19):10430–5.

1060 50. Lando D, Peet DJ, Gorman JJ, Whelan DA, Whitelaw ML, Bruick RK. FIH-1 is an
1061 asparaginyl hydroxylase enzyme that regulates the transcriptional activity of
1062 hypoxia-inducible factor. Genes Dev. 2002 Jun 15;16(12):1466–71.

1063 51. Prabhakar NR, Semenza GL. ADAPTIVE AND MALADAPTIVE
1064 CARDIORESPIRATORY RESPONSES TO CONTINUOUS AND INTERMITTENT
1065 HYPOXIA MEDIATED BY HYPOXIA-INDUCIBLE FACTORS 1 AND 2. Physiol Rev.
1066 2012 Jul;92(3):967–1003.

1067 52. Semenza GL. HIF-1 and mechanisms of hypoxia sensing. Current Opinion in
1068 Cell Biology. 2001 Apr 1;13(2):167–71.

1069 53. Prabhakar NR, Semenza GL. Adaptive and Maladaptive Cardiorespiratory
1070 Responses to Continuous and Intermittent Hypoxia Mediated by Hypoxia-
1071 Inducible Factors 1 and 2. Physiological Reviews. 2012 Jul;92(3):967–1003.

1072 54. Koh MY, Lemos R, Liu X, Powis G. The Hypoxia-Associated Factor Switches Cells
1073 from HIF-1α– to HIF-2α–Dependent Signaling Promoting Stem Cell
1074 Characteristics, Aggressive Tumor Growth and Invasion. Cancer Res. 2011 Jun
1075 1;71(11):4015–27.

1076 55. Makino Y, Uenishi R, Okamoto K, Isoe T, Hosono O, Tanaka H, et al.
1077 Transcriptional Up-regulation of Inhibitory PAS Domain Protein Gene Expression
1078 by Hypoxia-inducible Factor 1 (HIF-1): A NEGATIVE FEEDBACK REGULATORY
1079 CIRCUIT IN HIF-1-MEDIATED SIGNALING IN HYPOXIC CELLS. Journal of
1080 Biological Chemistry. 2007 May 11;282(19):14073–82.

1081 56. Duan C. Hypoxia-inducible factor 3 biology: complexities and emerging
1082 themes. Am J Physiol Cell Physiol. 2016 Feb 15;310(4):C260-269.

1083 57. Li QF, Wang XR, Yang YW, Lin H. Hypoxia upregulates hypoxia inducible factor
1084 (HIF)-3α expression in lung epithelial cells: characterization and comparison
1085 with HIF-1α. Cell Res. 2006 Jun;16(6):548–58.

1086 58. Main AM, Gillberg L, Jacobsen AL, Nilsson E, Gjesing AP, Hansen T, et al. DNA
1087 methylation and gene expression of HIF3A: cross-tissue validation and
1088 associations with BMI and insulin resistance. Clin Epigenetics. 2016 Sep
1089 2;8(1):89.

1090 59. Benita Y, Kikuchi H, Smith AD, Zhang MQ, Chung DC, Xavier RJ. An integrative
1091 genomics approach identifies Hypoxia Inducible Factor-1 (HIF-1)-target genes
1092 that form the core response to hypoxia. Nucleic Acids Res. 2009
1093 Aug;37(14):4587–602.

1094 60. Wang V, Davis DA, Haque M, Huang LE, Yarchoan R. Differential Gene Up-
1095 Regulation by Hypoxia-Inducible Factor-1α and Hypoxia-Inducible Factor-2α in
1096 HEK293T Cells. Cancer Research. 2005 Apr 15;65(8):3299–306.

1097 61. Manalo DJ, Rowan A, Lavoie T, Natarajan L, Kelly BD, Ye SQ, et al.
1098 Transcriptional regulation of vascular endothelial cell responses to hypoxia by
1099 HIF-1. Blood. 2005 Jan 15;105(2):659–69.

1100 62. Zhang L, Huang G, Li X, Zhang Y, Jiang Y, Shen J, et al. Hypoxia induces
1101 epithelial-mesenchymal transition via activation of SNAI1 by hypoxia-inducible
1102 factor -1α in hepatocellular carcinoma. BMC Cancer. 2013 Mar 9;13:108.

1103 63. Zhang W, Shi X, Peng Y, Wu M, Zhang P, Xie R, et al. HIF-1α Promotes
1104 Epithelial-Mesenchymal Transition and Metastasis through Direct Regulation of
1105 ZEB1 in Colorectal Cancer. PLOS ONE. 2015 Jun 9;10(6):e0129603.

1106 64. Schödel J, Oikonomopoulos S, Ragoussis J, Pugh CW, Ratcliffe PJ, Mole DR.
1107 High-resolution genome-wide mapping of HIF-binding sites by ChIP-seq. Blood.
1108 2011 Jun 9;117(23):e207–17.

1109 65. Morikawa M, Koinuma D, Miyazono K, Heldin CH. Genome-wide mechanisms of
1110 Smad binding. Oncogene. 2013 Mar;32(13):1609–15.

1111 66. Mallikarjuna P, Sitaram RT, Landström M, Ljungberg B. VHL status regulates
1112 transforming growth factor-β signaling pathways in renal cell carcinoma.
1113 Oncotarget. 2018 Mar 27;9(23):16297–310.

1114 67. Dai Y, Siemann D. c-Src is required for hypoxia-induced metastasis-associated
1115 functions in prostate cancer cells. Onco Targets Ther. 2019 May 8;12:3519–29.

1116 68. Guo Q, Lu L, Liao Y, Wang X, Zhang Y, Liu Y, et al. Influence of c-Src on hypoxic
1117 resistance to paclitaxel in human ovarian cancer cells and reversal of FV-429.
1118 Cell Death Dis. 2018 Jan;8(1):e3178–e3178.

1119 69. Lee G, Won HS, Lee YM, Choi JW, Oh TI, Jang JH, et al. Oxidative Dimerization
1120 of PHD2 is Responsible for its Inactivation and Contributes to Metabolic
1121 Reprogramming via HIF-1α Activation. Sci Rep. 2016 Jan 7;6(1):18928.

1122 70. Hu X, Wu X, Xu J, Zhou J, Han X, Guo J. Src kinase up-regulates the ERK
1123 cascade through inactivation of protein phosphatase 2A following cerebral
1124 ischemia. BMC Neurosci. 2009 Jul 14;10:74.

1125 71. Owens DW, McLean GW, Wyke AW, Paraskeva C, Parkinson EK, Frame MC, et al.
1126 The Catalytic Activity of the Src Family Kinases Is Required to Disrupt
1127 Cadherin-dependent Cell–Cell Contacts. MBoC. 2000 Jan;11(1):51–64.

1128 72. Zhang X, Guo J, Jabbarzadeh Kaboli P, Zhao Q, Xiang S, Shen J, et al. Analysis
1129 of Key Genes Regulating the Warburg Effect in Patients with Gastrointestinal
1130 Cancers and Selective Inhibition of This Metabolic Pathway in Liver Cancer
1131 Cells. Onco Targets Ther. 2020 Jul 27;13:7295–304.

1132 73. Goda N, Ryan HE, Khadivi B, McNulty W, Rickert RC, Johnson RS. Hypoxia-
1133 Inducible Factor 1α Is Essential for Cell Cycle Arrest during Hypoxia. Mol Cell
1134 Biol. 2003 Jan;23(1):359–69.

1135 74. Koshiji M, Kageyama Y, Pete EA, Horikawa I, Barrett JC, Huang LE. HIF-1α
1136 induces cell cycle arrest by functionally counteracting Myc. EMBO J. 2004 May
1137 5;23(9):1949–56.

1138 75. Chen Y, Yan H, Yan L, Wang X, Che X, Hou K, et al. Hypoxia-induced ALDH3A1
1139 promotes the proliferation of non-small-cell lung cancer by regulating energy
1140 metabolism reprogramming. Cell Death Dis. 2023 Sep 20;14(9):1–11.

1141 76. Whelan KA, Caldwell SA, Shahriari KS, Jackson SR, Franchetti LD, Johannes GJ,
1142 et al. Hypoxia Suppression of Bim and Bmf Blocks Anoikis and Luminal Clearing
1143 during Mammary Morphogenesis. Mol Biol Cell. 2010 Nov 15;21(22):3829–37.

1144 77. Rohwer N, Welzel M, Daskalow K, Pfander D, Wiedenmann B, Detjen K, et al.
1145 Hypoxia-Inducible Factor 1α Mediates Anoikis Resistance via Suppression of α5
1146 Integrin. Cancer Research. 2008 Dec 15;68(24):10113–20.

1147 78. Saikumar P, Dong Z, Patel Y, Hall K, Hopfer U, Weinberg JM, et al. Role of
1148 hypoxia-induced Bax translocation and cytochrome c release in reoxygenation
1149 injury. Oncogene. 1998 Dec;17(26):3401–15.

1150 79. Greijer AE, van der Wall E. The role of hypoxia inducible factor 1 (HIF-1) in
1151 hypoxia induced apoptosis. J Clin Pathol. 2004 Oct;57(10):1009–14.

1152 80. Dong Z, Venkatachalam MA, Wang J, Patel Y, Saikumar P, Semenza GL, et al.
1153 Up-regulation of apoptosis inhibitory protein IAP-2 by hypoxia. Hif-1-
1154 independent mechanisms. J Biol Chem. 2001 Jun 1;276(22):18702–9.

1155 81. Dagogo-Jack I, Shaw AT. Tumour heterogeneity and resistance to cancer
1156 therapies. Nat Rev Clin Oncol. 2018 Feb;15(2):81–94.

1157 82. Jacquemin V, Antoine M, Dom G, Detours V, Maenhaut C, Dumont JE. Dynamic
1158 Cancer Cell Heterogeneity: Diagnostic and Therapeutic Implications. Cancers
1159 (Basel). 2022 Jan 7;14(2):280.

1160 83. Simeonov KP, Byrns CN, Clark ML, Norgard RJ, Martin B, Stanger BZ, et al.
1161 Single-cell lineage tracing of metastatic cancer reveals selection of hybrid EMT
1162 states. Cancer Cell. 2021 Aug 9;39(8):1150-1162.e9.

1163 84. Zhang Q, Fei L, Han R, Huang R, Wang Y, Chen H, et al. Single-cell
1164 transcriptome reveals cellular hierarchies and guides p-EMT-targeted trial in
1165 skull base chordoma. Cell Discov. 2022 Sep 20;8(1):94.

1166 85. Sullivan E, Harris M, Bhatnagar A, Guberman E, Zonfa I, Ravasz Regan E.
1167 Boolean modeling of mechanosensitive epithelial to mesenchymal transition
1168 and its reversal. iScience. 2023 Apr 21;26(4):106321.

1169 86. Schwab LP, Peacock DL, Majumdar D, Ingels JF, Jensen LC, Smith KD, et al.
1170 Hypoxia-inducible factor 1α promotes primary tumor growth and tumor-
1171 initiating cell activity in breast cancer. Breast Cancer Research. 2012 Jan
1172 7;14(1):R6.

1173 87. D'Uva G, Bertoni S, Lauriola M, De Carolis S, Pacilli A, D'Anello L, et al. Beta-
1174 Catenin/HuR Post-Transcriptional Machinery Governs Cancer Stem Cell Features
1175 in Response to Hypoxia. PLoS One. 2013 Nov 15;8(11):e80742.

1176 88. Yang MH, Wu MZ, Chiou SH, Chen PM, Chang SY, Liu CJ, et al. Direct regulation
1177 of TWIST by HIF-1alpha promotes metastasis. Nat Cell Biol. 2008
1178 Mar;10(3):295–305.

1179 89. Lv Y, Chen C, Zhao B, Zhang X. Regulation of matrix stiffness on the epithelial-
1180 mesenchymal transition of breast cancer cells under hypoxia environment.
1181 Naturwissenschaften. 2017 Jun;104(5–6):38.

1182 90. Uchida T, Rossignol F, Matthay MA, Mounier R, Couette S, Clottes E, et al.
1183 Prolonged Hypoxia Differentially Regulates Hypoxia-inducible Factor (HIF)-1α
1184 and HIF-2α Expression in Lung Epithelial Cells: IMPLICATION OF NATURAL
1185 ANTISENSE HIF-1α*. Journal of Biological Chemistry. 2004 Apr
1186 9;279(15):14871–8.

91. Kaidi A, Williams AC, Paraskeva C. Interaction between beta-catenin and HIF-1 promotes cellular adaptation to hypoxia. Nat Cell Biol. 2007 Feb;9(2):210–7.

92. Yeung SJ, Pan J, Lee MH. Roles of p53, Myc and HIF-1 in Regulating Glycolysis — the Seventh Hallmark of Cancer. Cell Mol Life Sci. 2008 Sep 3;65(24):3981.

93. Horváthová J, Moravčík R, Matúšková M, Šišovský V, Boháč A, Zeman M. Inhibition of Glycolysis Suppresses Cell Proliferation and Tumor Progression In Vivo: Perspectives for Chronotherapy. Int J Mol Sci. 2021 Apr 22;22(9):4390.

94. Belapurkar R, Pfisterer M, Dreute J, Werner S, Zukunft S, Fleming I, et al. A transient increase of HIF-1α during the G1 phase (G1-HIF) ensures cell survival under nutritional stress. Cell Death Dis. 2023 Jul 27;14(7):1–15.

95. Green SL, Freiberg RA, Giaccia AJ. p21(Cip1) and p27(Kip1) regulate cell cycle reentry after hypoxic stress but are not necessary for hypoxia-induced arrest. Mol Cell Biol. 2001 Feb;21(4):1196–206.

96. Luo Y, Li M, Zuo X, Basourakos SP, Zhang J, Zhao J, et al. β-catenin nuclear translocation induced by HIF-1α overexpression leads to the radioresistance of prostate cancer. Int J Oncol. 2018 Jun;52(6):1827–40.

97. Cummins EP, Berra E, Comerford KM, Ginouves A, Fitzgerald KT, Seeballuck F, et al. Prolyl hydroxylase-1 negatively regulates IκB kinase-β, giving insight into hypoxia-induced NFκB activity. Proc Natl Acad Sci U S A. 2006 Nov 28;103(48):18154–9.

98. McMahon S, Grondin F, McDonald PP, Richard DE, Dubois CM. Hypoxia-enhanced expression of the proprotein convertase furin is mediated by hypoxia-inducible factor-1: impact on the bioactivation of proproteins. J Biol Chem. 2005 Feb 25;280(8):6561–9.

99. Matsuoka J, Yashiro M, Doi Y, Fuyuhiro Y, Kato Y, Shinto O, et al. Hypoxia Stimulates the EMT of Gastric Cancer Cells through Autocrine TGFβ Signaling. PLOS ONE. 2013 May 17;8(5):e62310.

100. Mallikarjuna P, Raviprakash TS, Aripaka K, Ljungberg B, Landström M. Interactions between TGF-β type I receptor and hypoxia-inducible factor-α mediates a synergistic crosstalk leading to poor prognosis for patients with clear cell renal cell carcinoma. Cell Cycle. 2019 Jul 24;18(17):2141–56.

101. Brereton CJ, Yao L, Davies ER, Zhou Y, Vukmirovic M, Bell JA, et al. Pseudohypoxic HIF pathway activation dysregulates collagen structure-function in human lung fibrosis. eLife. 11:e69348.

102. Muñoz-Nájar UM, Neurath KM, Vumbaca F, Claffey KP. Hypoxia stimulates breast carcinoma cell invasion through MT1-MMP and MMP-2 activation. Oncogene. 2006 Apr 13;25(16):2379–92.

1224 103. Choi JY, Jang YS, Min SY, Song JY. Overexpression of MMP-9 and HIF-1α in
1225 Breast Cancer Cells under Hypoxic Conditions. J Breast Cancer. 2011
1226 Jun;14(2):88–95.

1227 104. Park JS, Burckhardt CJ, Lazcano R, Solis LM, Isogai T, Li L, et al. Mechanical
1228 regulation of glycolysis via cytoskeleton architecture. Nature. 2020
1229 Feb;578(7796):621–6.

1230 105. Gizak A, Wiśniewski J, Heron P, Mamczur P, Sygusch J, Rakus D. Targeting a
1231 moonlighting function of aldolase induces apoptosis in cancer cells. Cell Death
1232 Dis. 2019 Sep 26;10(10):712.

1233 106. van Leeuwaarde RS, Ahmad S, van Nesselrooij B, Zandee W, Giles RH. Von
1234 Hippel-Lindau Syndrome. In: Adam MP, Feldman J, Mirzaa GM, Pagon RA,
1235 Wallace SE, Bean LJ, et al., editors. GeneReviews® [Internet]. Seattle (WA):
1236 University of Washington, Seattle; 1993 [cited 2024 Jan 25]. Available from:
1237 http://www.ncbi.nlm.nih.gov/books/NBK1463/

1238 107. Ferlay J, Colombet M, Soerjomataram I, Dyba T, Randi G, Bettio M, et al.
1239 Cancer incidence and mortality patterns in Europe: Estimates for 40 countries
1240 and 25 major cancers in 2018. Eur J Cancer. 2018 Nov;103:356–87.

1241 108. Clark PE. The role of VHL in clear-cell renal cell carcinoma and its relation to
1242 targeted therapy. Kidney International. 2009 Nov 1;76(9):939–45.

1243 109. Pritchett TL, Bader HL, Henderson J, Hsu T. Conditional inactivation of the
1244 mouse von Hippel–Lindau tumor suppressor gene results in wide-spread
1245 hyperplastic, inflammatory and fibrotic lesions in the kidney. Oncogene. 2015
1246 May;34(20):2631–9.

1247 110. Wang SS, Gu YF, Wolff N, Stefanius K, Christie A, Dey A, et al. Bap1 is essential
1248 for kidney function and cooperates with Vhl in renal tumorigenesis. Proceedings
1249 of the National Academy of Sciences. 2014 Nov 18;111(46):16538–43.

1250 111. Xu Z, Liu L, Jiang W, Qiu Y, Zhang B, Cheng J, et al. VHL missense mutation
1251 delineate aggressive clear cell renal cell carcinoma subtype with favorable
1252 immunotherapeutic response. J Immunother Cancer. 2024 Oct
1253 23;12(10):e009963.

1254 112. Gordan JD, Lal P, Dondeti VR, Letrero R, Parekh KN, Oquendo CE, et al. HIF-α
1255 Effects on c-Myc Distinguish Two Subtypes of Sporadic VHL-Deficient Clear Cell
1256 Renal Carcinoma. Cancer Cell. 2008 Dec 9;14(6):435–46.

1257 113. Lin PH, Huang CY, Yu KJ, Kan HC, Liu CY, Chuang CK, et al. Genomic
1258 characterization of clear cell renal cell carcinoma using targeted gene
1259 sequencing. Oncol Lett. 2021 Feb;21(2):169.

114. Adeshakin FO, Adeshakin AO, Afolabi LO, Yan D, Zhang G, Wan X. Mechanisms for Modulating Anoikis Resistance in Cancer and the Relevance of Metabolic Reprogramming. Front Oncol. 2021 Mar 29;11:626577.

115. Dong Z, Wang JZ, Yu F, Venkatachalam MA. Apoptosis-Resistance of Hypoxic Cells. Am J Pathol. 2003 Aug;163(2):663–71.

116. Park SH, Riley P, Frisch SM. Regulation of anoikis by Deleted in Breast Cancer-1 (DBC1) through NF-κB. Apoptosis. 2013 Aug;18(8):949–62.

117. Wang CY, Guttridge DC, Mayo MW, Baldwin AS. NF-κB Induces Expression of the Bcl-2 Homologue A1/Bfl-1 To Preferentially Suppress Chemotherapy-Induced Apoptosis. Mol Cell Biol. 1999 Sep;19(9):5923–9.

118. Tilghman RW, Cowan CR, Mih JD, Koryakina Y, Gioeli D, Slack-Davis JK, et al. Matrix Rigidity Regulates Cancer Cell Growth and Cellular Phenotype. PLOS ONE. 2010 Sep 23;5(9):e12905.

119. Mittal V. Epithelial Mesenchymal Transition in Tumor Metastasis. Annu Rev Pathol. 2018 Jan 24;13:395–412.

120. Deritei D, Anamika WJ, Zhou X, Silverman EK, Regan ER, Glass K. HHIP's Dynamic Role in Epithelial Wound Healing Reveals a Potential Mechanism of COPD Susceptibility [Internet]. bioRxiv; 2024 [cited 2024 Dec 18]. p. 2024.09.05.611545. Available from: https://www.biorxiv.org/content/10.1101/2024.09.05.611545v2

121. Kai F, Drain AP, Weaver VM. The extracellular matrix modulates the metastatic journey. Dev Cell. 2019 May 6;49(3):332–46.

122. Nguyen LK, Cavadas MAS, Scholz CC, Fitzpatrick SF, Bruning U, Cummins EP, et al. A dynamic model of the hypoxia-inducible factor 1α (HIF-1α) network. Journal of Cell Science. 2013 Mar 15;126(6):1454–63.

123. Qutub AA, Popel AS. A computational model of intracellular oxygen sensing by hypoxia-inducible factor HIF1α. J Cell Sci. 2006 Aug 15;119(Pt 16):3467–80.

124. Hashemzadeh S, Shahmorad S, Rafii-Tabar H, Omidi Y. Computational modeling to determine key regulators of hypoxia effects on the lactate production in the glycolysis pathway. Sci Rep. 2020 Jun 8;10(1):9163.

125. Oliveira RH de M, Annex BH, Popel AS. Endothelial cells signaling and patterning under hypoxia: a mechanistic integrative computational model including the Notch-Dll4 pathway. Front Physiol [Internet]. 2024 Feb 22 [cited 2024 Dec 18];15. Available from: https://www.frontiersin.org/journals/physiology/articles/10.3389/fphys.2024.1351753/full

126. Hanahan D. Hallmarks of Cancer: New Dimensions. Cancer Discovery. 2022 Jan 12;12(1):31–46.

127. Kierans SJ, Taylor CT. Regulation of glycolysis by the hypoxia-inducible factor (HIF): implications for cellular physiology. The Journal of Physiology. 2021;599(1):23–37.

128. Gordan JD, Bertovrt JA, Hu CJ, Diehl JA, Simon MC. HIF-2α promotes hypoxic cell proliferation by enhancing c-Myc transcriptional activity. Cancer Cell. 2007 Apr;11(4):335–47.

129. Zhu C, Yu J, Pan Q, Yang J, Hao G, Wang Y, et al. Hypoxia-inducible factor-2 alpha promotes the proliferation of human placenta-derived mesenchymal stem cells through the MAPK/ERK signaling pathway. Sci Rep. 2016 Oct 21;6(1):35489.

130. Ma X, Zhang H, Xue X, Shah YM. Hypoxia-inducible factor 2α (HIF-2α) promotes colon cancer growth by potentiating Yes-associated protein 1 (YAP1) activity. Journal of Biological Chemistry. 2017 Oct 13;292(41):17046–56.

131. Chen SH, Xu LY, Wu YP, Ke ZB, Huang P, Lin F, et al. Tumor volume: a new prognostic factor of oncological outcome of localized clear cell renal cell carcinoma. BMC Cancer. 2021 Jan 19;21(1):79.

132. Chrabańska M, Szweda-Gandor N, Drozdzowska B. Two Single Nucleotide Polymorphisms in the Von Hippel-Lindau Tumor Suppressor Gene in Patients with Clear Cell Renal Cell Carcinoma. Int J Mol Sci. 2023 Feb 14;24(4):3778.

133. Stone RC, Pastar I, Ojeh N, Chen V, Liu S, Garzon KI, et al. Epithelial-Mesenchymal Transition in Tissue Repair and Fibrosis. Cell Tissue Res. 2016 Sep;365(3):495–506.

134. Lin Q, Cong X, Yun Z. Differential hypoxic regulation of hypoxia-inducible factors 1α and 2α. Mol Cancer Res. 2011 Jun;9(6):757–65.

135. Zhang P, Yao Q, Lu L, Li Y, Chen PJ, Duan C. Hypoxia-Inducible Factor 3 Is an Oxygen-Dependent Transcription Activator and Regulates a Distinct Transcriptional Response to Hypoxia. Cell Reports. 2014 Mar 27;6(6):1110–21.

136. Augstein A, Poitz DM, Braun-Dullaeus RC, Strasser RH, Schmeisser A. Cell-specific and hypoxia-dependent regulation of human HIF-3α: inhibition of the expression of HIF target genes in vascular cells. Cell Mol Life Sci. 2011 Aug 1;68(15):2627–42.

137. Sizek H, Deritei D, Fleig K, Harris M, Regan PL, Glass K, et al. Unlocking Mitochondrial Dysfunction-Associated Senescence (MiDAS) with NAD+ – a Boolean Model of Mitochondrial Dynamics and Cell Cycle Control. Tansl Onc. 2023 Dec 1;(submitted).

138. Kang H, Kim H, Lee S, Youn H, Youn B. Role of Metabolic Reprogramming in Epithelial–Mesenchymal Transition (EMT). Int J Mol Sci. 2019 Apr 25;20(8):2042.

139. Hong CF, Chen WY, Wu CW. Upregulation of Wnt signaling under hypoxia promotes lung cancer progression. Oncol Rep. 2017 Sep;38(3):1706–14.

140. Shen X, Li M, Wang C, Liu Z, Wu K, Wang A, et al. Hypoxia is fine-tuned by Hif-1α and regulates mesendoderm differentiation through the Wnt/β-Catenin pathway. BMC Biol. 2022 Oct 5;20(1):219.

141. Guo M, Niu Y, Xie M, Liu X, Li X. Notch signaling, hypoxia, and cancer. Front Oncol. 2023 Jan 31;13:1078768.

142. Gyamfi J, Lee YH, Eom M, Choi J. Interleukin-6/STAT3 signalling regulates adipocyte induced epithelial-mesenchymal transition in breast cancer cells. Sci Rep. 2018 Jun 11;8:8859.

143. Zhang T, Yang J, Sun Y, Song J, Gao D, Huang S, et al. Interleukin-6 and Hypoxia Synergistically Promote EMT-Mediated Invasion in Epithelial Ovarian Cancer via the IL-6/STAT3/HIF-1α Feedback Loop. Anal Cell Pathol (Amst). 2023 Feb 13;2023:8334881.

144. Li X, Kimura H, Hirota K, Kasuno K, Torii K, Okada T, et al. Synergistic effect of hypoxia and TNF-α on production of PAI-1 in human proximal renal tubular cells. Kidney International. 2005 Aug 1;68(2):569–83.

145. Basu S, Cheriyamundath S, Ben-Ze'ev A. Cell–cell adhesion: linking Wnt/β-catenin signaling with partial EMT and stemness traits in tumorigenesis. F1000Res. 2018 Sep 18;7:F1000 Faculty Rev-1488.

146. Katoh Y, Katoh M. Hedgehog signaling, epithelial-to-mesenchymal transition and miRNA (review). Int J Mol Med. 2008 Sep;22(3):271–5.

147. Deshmukh AP, Vasaikar SV, Tomczak K, Tripathi S, den Hollander P, Arslan E, et al. Identification of EMT signaling cross-talk and gene regulatory networks by single-cell RNA sequencing. Proceedings of the National Academy of Sciences. 2021 May 11;118(19):e2102050118.

148. Shaul ME, Fridlender ZG. Tumour-associated neutrophils in patients with cancer. Nat Rev Clin Oncol. 2019 Oct;16(10):601–20.

149. Doak GR, Schwertfeger KL, Wood DK. Distant Relations: Macrophage Functions in the Metastatic Niche. Trends in Cancer. 2018 Jun 1;4(6):445–59.

150. Schlesinger M. Role of platelets and platelet receptors in cancer metastasis. J Hematol Oncol. 2018 Oct 11;11(1):125.

151. Gaggioli C, Hooper S, Hidalgo-Carcedo C, Grosse R, Marshall JF, Harrington K, et al. Fibroblast-led collective invasion of carcinoma cells with differing roles for RhoGTPases in leading and following cells. Nat Cell Biol. 2007 Dec;9(12):1392–400.

152. Guo Y, Cui W, Pei Y, Xu D. Platelets promote invasion and induce epithelial to mesenchymal transition in ovarian cancer cells by TGF-β signaling pathway. Gynecologic Oncology. 2019 Jun;153(3):639–50.

153. Nacarelli T, Lau L, Fukumoto T, Zundell J, Fatkhutdinov N, Wu S, et al. NAD+ metabolism governs the proinflammatory senescence-associated secretome. Nat Cell Biol. 2019 Mar;21(3):397–407.

154. Smit MA, Peeper DS. Epithelial-mesenchymal transition and senescence: two cancer-related processes are crossing paths. Aging (Albany NY). 2010 Oct 17;2(10):735–41.

155. Liu Y, El-Naggar S, Darling DS, Higashi Y, Dean DC. ZEB1 Links Epithelial-Mesenchymal Transition and Cellular Senescence. Development. 2008 Feb;135(3):579–88.

156. Malik-Sheriff RS, Glont M, Nguyen TVN, Tiwari K, Roberts MG, Xavier A, et al. BioModels-15 years of sharing computational models in life science. Nucleic Acids Res. 2020 Jan 8;48(D1):D407–15.

157. Chaouiya C, Naldi A, Thieffry D. Logical modelling of gene regulatory networks with GINsim. Methods Mol Biol. 2012;804:463–79.

158. Helikar T, Kowal B, McClenathan S, Bruckner M, Rowley T, Madrahimov A, et al. The Cell Collective: toward an open and collaborative approach to systems biology. BMC Syst Biol. 2012 Aug 7;6:96.

159. Albert I, Thakar J, Li S, Zhang R, Albert R. Boolean network simulations for life scientists. Source Code Biol Med. 2008 Nov 14;3:16.

160. yWorks GmbH. yEd [Internet]. 2019. Available from: https://www.yworks.com/products/yed

161. Mann M, Klemm K. Efficient exploration of discrete energy landscapes. Physical Review E. 2009 Oct;83(1):011113.

162. Deritei D, Aird WC, Ercsey-Ravasz M, Regan ER. Principles of dynamical modularity in biological regulatory networks. Sci Rep. 2016 Mar 16;6:21957.

163. Sizek H, Hamel A, Deritei D, Campbell S, Ravasz Regan E. Boolean model of growth signaling, cell cycle and apoptosis predicts the molecular mechanism of aberrant cell cycle progression driven by hyperactive PI3K. PLoS Comput Biol. 2019;15(3):e1006402.

164. Guberman E, Sherief H, Regan ER. Boolean model of anchorage dependence and contact inhibition points to coordinated inhibition but semi-independent induction of proliferation and migration. Comput Struct Biotechnol J. 2020;18:2145–65.

Supplementary Figures

SM Figure 1. Hif-1□ is required for proliferation under normoxia (full version of Fig. 2A).

SM Figure 2. Hif-1□ hyper-activation blocks the cell cycle by repressing Myc.

SM Figure 3. Hypoxia induces EMT independently of TFG-β.

SM Figure 4. A stiff ECM aids hypoxia-induced EMT, compared to hybrid E/M under normoxia.

SM Figure 5. ECM stiffness boosts both hypoxia- and TGF-β-induced EMT; high levels of both are required to drive EMT on very soft ECMs.

SM Figure 6. VHL deficiency boosts bio mechanically induced EMT in normoxia as well as hypoxia at moderate ECM stiffness and medium-high density, but abolishes cell cycle entry.

SM Figure 7. VHL deficiency-induced cell cycle arrest is broken by cooperative hyper-activation of Myc and Cyclin D.

SM Figure 8. Hypoxia confers anoikis resistance and protection from TGF-β induced epithelial cell apoptosis on a soft ECM (full version of Fig. 5).

SM Figure 9. Saturating autocrine TGF-β signaling protects all mesenchymal cells from anoikis, but also blocks MET on a stiff ECM.

SM Figure 10. Slight breaks in the autocrine TGF-β signaling loop are potent inducers of anoikis and apoptosis on soft ECM.

SM Figure 11. A changing mix of model cell phenotypes as a function of mitogen, cell density, ECM stiffness and hypoxia allows us to track TME-driven EMT and MET during the metastatic cascade.

Supplementary Tables

SM Table 1. Description and experimental support for all nodes and links of the Boolean Regulatory network model in Fig. 1C.

SM Table 2. List of 150 published experimental assays used for model validation, marked to indicate success/failure of the model in replicating each assay.

Supplementary Files

SM File 1. Files read by *dynmod* to simulate the Boolean model's behaviors. These include the model in .dmms format (as well as .BooleanNet and .SBML formats, namely *Hypoxia_EMT_Model.dmms*, *Hypoxia_EMT_Model.booleannet, Hypoxia_EMT_Model.sbml*), the "in silico protocol" files for reproducing all figures (*Hypoxia_EMT_Main_Fig.vex, Hypoxia_EMT_SM_Fig.vex*) and the model network in .graphml format (*Hypoxia_EMT_Model.graphml*).

SM File 2. Files read by *dynmod* to simulate the isolated EMT module. These include the EMT module model in .dmms format (*EMT_module_Hypoxia.dmms*) and an "in silico protocol" file for generating time courses to check the module's attractors (*EMT_Module.vex*).

SM File 3. Files read by *dynmod* to rerun all model validation experiments (*Hypoxia_EMT_Validation.vex*), the Pyhton3 script and .csv file that performs statistical tests on the simulation results, summarizes them, and generates the figures SM File 4 (*Hypoxia Model Validation Script.py, ST2 - Hypoxia model validation list.csv*).

SM File 4. Auto-generated validation figures (150 panels with statistical tests, marked for match / mismatch with expediting data).

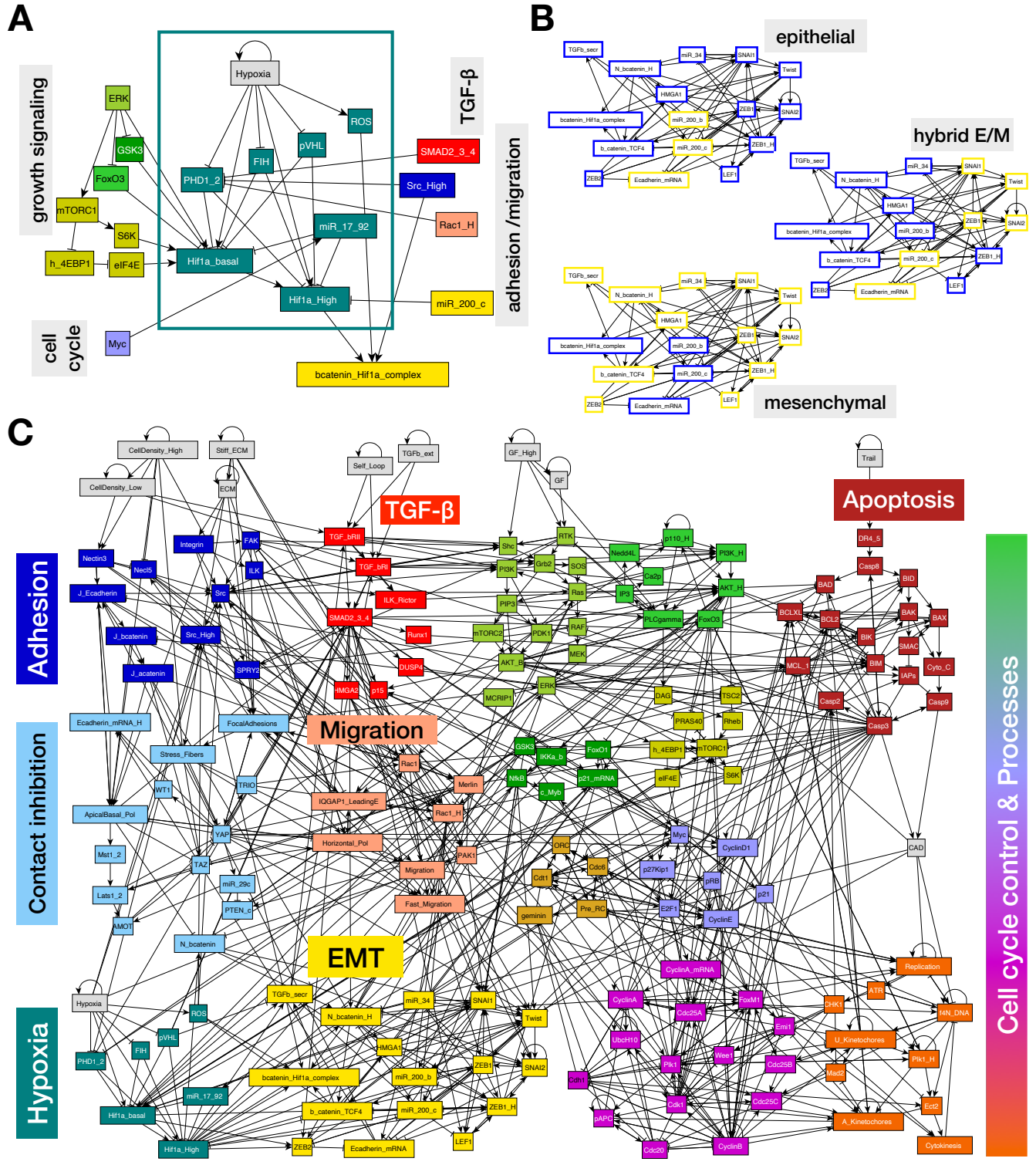
A
growth signaling
TGF-β
adhesion /migration
cell cycle
Hypoxia
ERK
GSK3
FoxO3
mTORC1
S6K
h_4EBP1
eIF4E
Hif1a_basal
Hif1a_High
Myc
ROS
pVHL
FIH
PHD1_2
SMAD2_3_4
Src_High
Rac1_H
miR_17_92
miR_200_c
bcatenin_Hif1a_complex
B
epithelial
hybrid E/M
mesenchymal
TGFb_secr
N_bcatenin_H
miR_34
SNAI1
Twist
HMGA1
ZEB1
SNAI2
bcatenin_Hif1a_complex
miR_200_b
b_catenin_TCF4
miR_200_c
ZEB1_H
ZEB2
Ecadherin_mRNA
LEF1
C
Adhesion
Contact inhibition
Hypoxia
Cell cycle control & Processes
TGF-β
Apoptosis
Migration
EMT
CellDensity_High
Stiff_ECM
Self_Loop
TGFb_ext
GF_High
GF
Trail
CellDensity_Low
ECM
Integrin
FAK
ILK
Nectin3
Necl5
J_Ecadherin
Src
J_bcatenin
Src_High
J_acatenin
SPRY2
TGF_bRII
TGF_bRI
ILK_Rictor
SMAD2_3_4
Runx1
DUSP4
HMGA2
p15
Shc
RTK
PI3K
Grb2
SOS
Ras
PIP3
mTORC2
PDK1
RAF
AKT_B
MEK
ERK
MCRIP1
Nedd4L
p110_H
PI3K_H
Ca2p
IP3
AKT_H
PLCgamma
FoxO3
DAG
TSC2
PRAS40
Rheb
DR4_5
Casp8
BID
BAD
BCLXL
BCL2
BAK
BAX
BIK
SMAC
MCL_1
BIM
IAPs
Cyto_C
Casp2
Casp9
Casp3
Ecadherin_mRNA_H
FocalAdhesions
Stress_Fibers
WT1
TRIO
Rac1
Merlin
IQGAP1_LeadingE
Rac1_H
GSK3
IKKa_b
FoxO1
h_4EBP1
mTORC1
NfkB
p21_mRNA
eIF4E
S6K
c_Myb
ApicalBasal_Pol
YAP
Horizontal_Pol
Myc
CyclinD1
CAD
Mst1_2
TAZ
PAK1
ORC
Cdc6
p27Kip1
Migration
Cdt1
pRB
p21
Lats1_2
miR_29c
PTEN_c
Fast_Migration
geminin
Pre_RC
E2F1
CyclinE
AMOT
N_bcatenin
CyclinA_mRNA
Replication
TGFb_secr
miR_34
SNAI1
CyclinA
FoxM1
ATR
CHK1
f4N_DNA
Hypoxia
ROS
N_bcatenin_H
Twist
Cdc25A
Emi1
pVHL
FIH
HMGA1
UbcH10
U_Kinetochores
PHD1_2
ZEB1
SNAI2
Plk1
Wee1
Cdc25B
Plk1_H
bcatenin_Hif1a_complex
miR_200_b
Cdh1
Mad2
miR_17_92
Cdk1
Cdc25C
Ect2
Hif1a_basal
b_catenin_TCF4
miR_200_c
ZEB1_H
pAPC
A_Kinetochores
Hif1a_High
ZEB2
Ecadherin_mRNA
LEF1
Cdc20
CyclinB
Cytokinesis

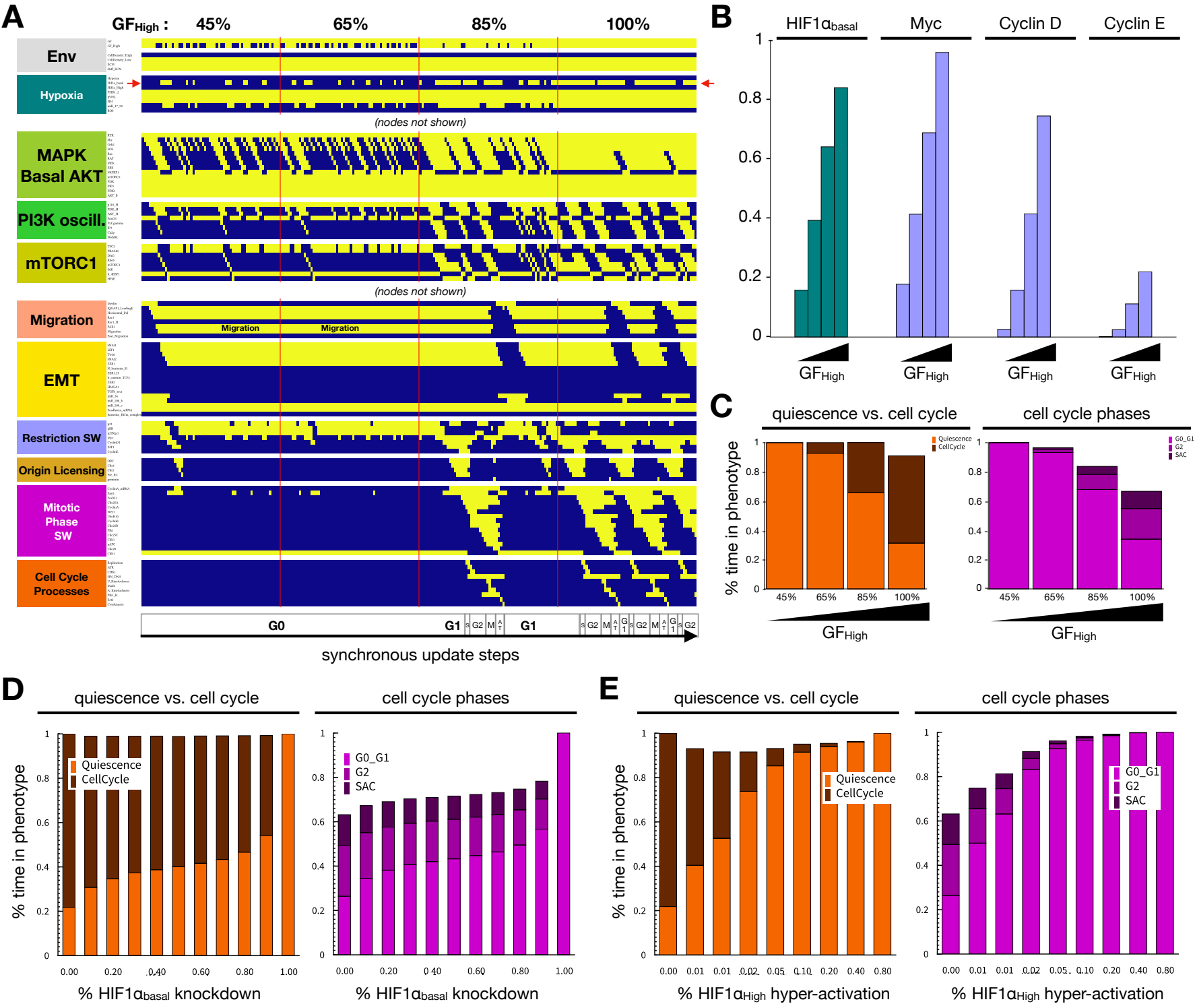
A
GF_High : 45% 65% 85% 100%
Env
Hypoxia
(nodes not shown)
MAPK Basal AKT
PI3K oscill.
mTORC1
(nodes not shown)
Migration
Migration
Migration
EMT
Restriction SW
Origin Licensing
Mitotic Phase SW
Cell Cycle Processes
G0
G1
S
G2
M
AT
G1
S
G2
M
AT
G1
S
G2
M
AT
G1
S
G2
synchronous update steps
B
HIF1αbasal
Myc
Cyclin D
Cyclin E
GF_High
C
quiescence vs. cell cycle
cell cycle phases
% time in phenotype
Quiescence
CellCycle
G0_G1
G2
SAC
45%
65%
85%
100%
GF_High
D
quiescence vs. cell cycle
cell cycle phases
% time in phenotype
Quiescence
CellCycle
G0_G1
G2
SAC
% HIF1αbasal knockdown
% HIF1αbasal knockdown
E
quiescence vs. cell cycle
cell cycle phases
% time in phenotype
Quiescence
CellCycle
G0_G1
G2
SAC
% HIF1αHigh hyper-activation
% HIF1αHigh hyper-activation

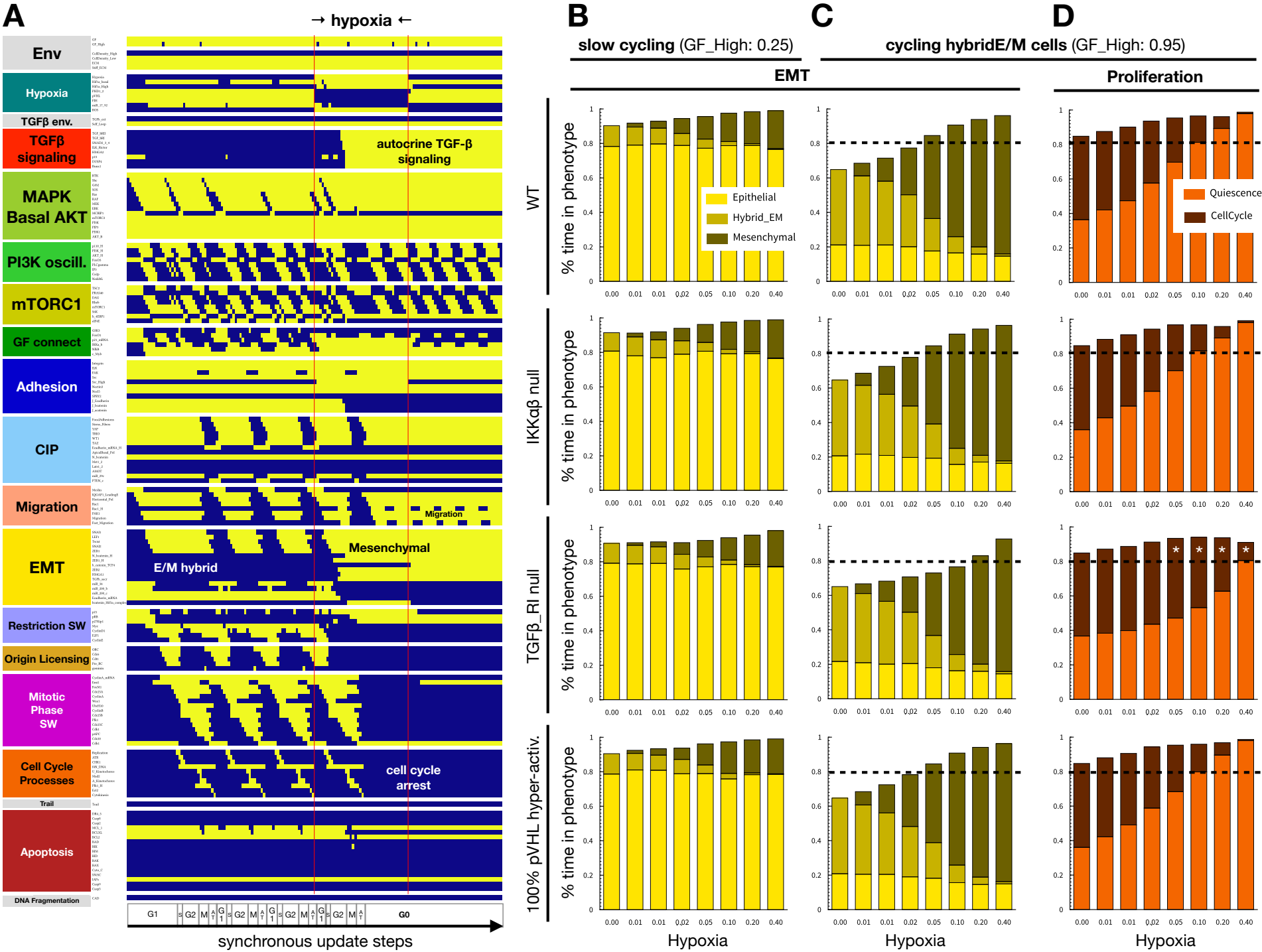
A
→ hypoxia ←
Env
Hypoxia
TGFβ env.
TGFβ signaling
autocrine TGF-β signaling
MAPK Basal AKT
PI3K oscill.
mTORC1
GF connect
Adhesion
CIP
Migration
Migration
EMT
Mesenchymal
E/M hybrid
Restriction SW
Origin Licensing
Mitotic Phase SW
Cell Cycle Processes
cell cycle arrest
Trail
Apoptosis
DNA Fragmentation
G1 S G2 M A G1 S G2 M A G1 S G2 M A G1 S G2 M A G0
synchronous update steps
B
slow cycling (GF_High: 0.25)
C
D
cycling hybridE/M cells (GF_High: 0.95)
EMT
Proliferation
WT
IKKαβ null
TGFβ_RI null
100% pVHL hyper-activ.
% time in phenotype
Epithelial
Hybrid_EM
Mesenchymal
Quiescence
CellCycle
0.00 0.01 0.01 0.02 0.05 0.10 0.20 0.40
Hypoxia

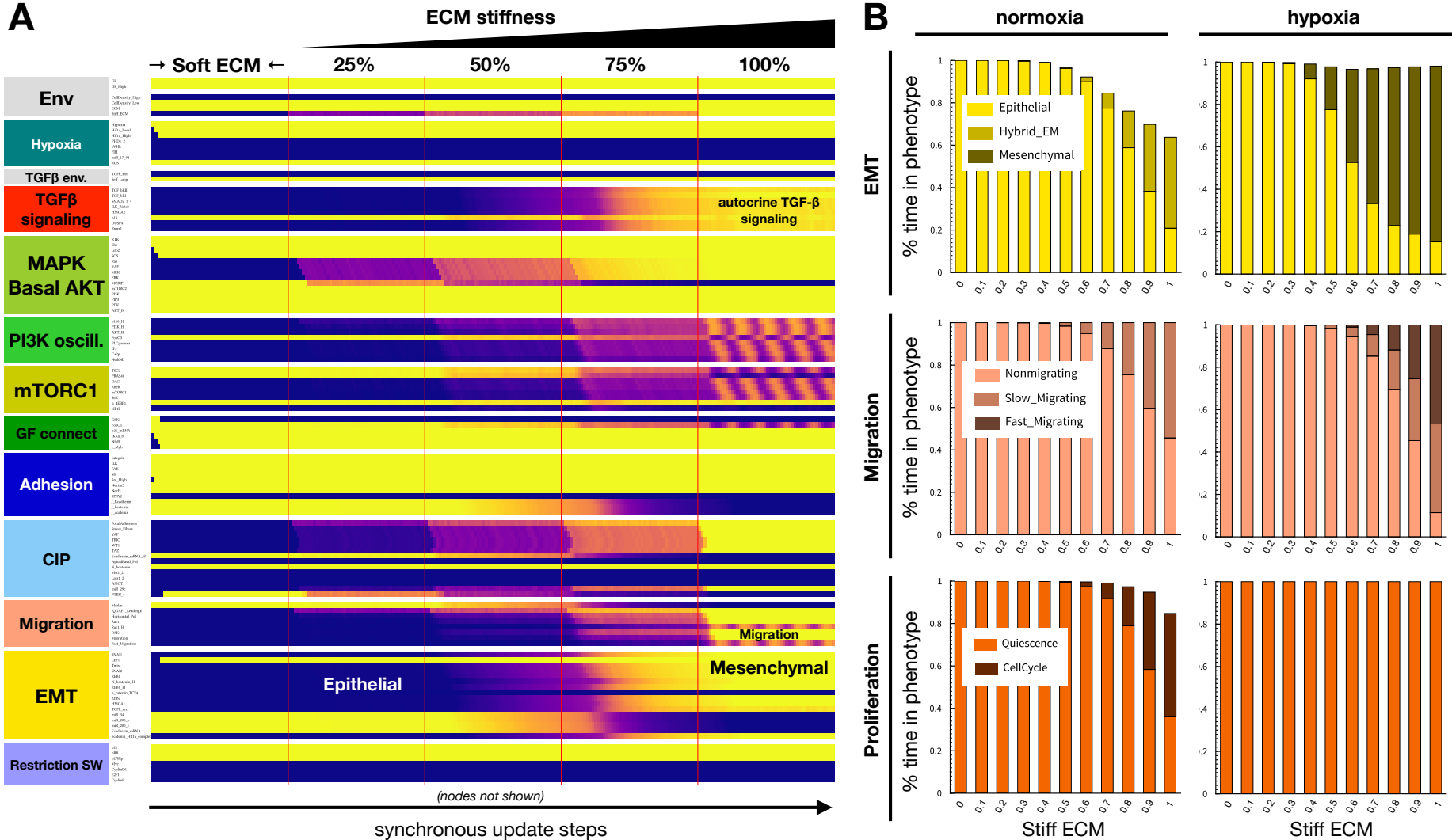
A
ECM stiffness
→ Soft ECM ←
25%
50%
75%
100%
Env
Hypoxia
TGFβ env.
TGFβ signaling
MAPK Basal AKT
PI3K oscill.
mTORC1
GF connect
Adhesion
CIP
Migration
EMT
Restriction SW
autocrine TGF-β signaling
Migration
Mesenchymal
Epithelial
(nodes not shown)
synchronous update steps
B
normoxia
hypoxia
EMT
Migration
Proliferation
% time in phenotype
Epithelial
Hybrid_EM
Mesenchymal
Nonmigrating
Slow_Migrating
Fast_Migrating
Quiescence
CellCycle
Stiff ECM
Stiff ECM

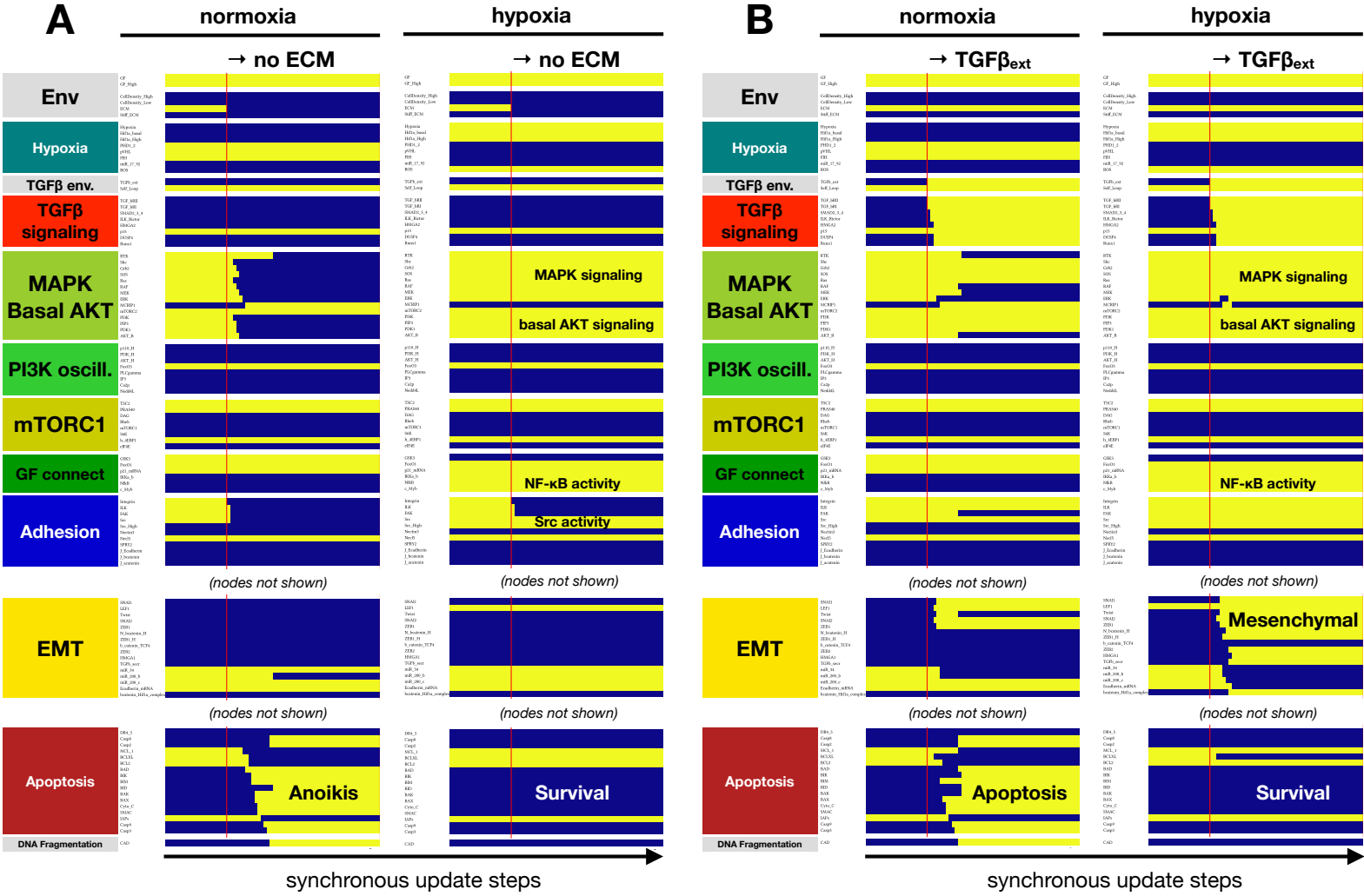
A
normoxia
hypoxia
→ no ECM
→ no ECM
B
normoxia
hypoxia
→ TGFβext
→ TGFβext
Env
Hypoxia
TGFβ env.
TGFβ signaling
MAPK Basal AKT
PI3K oscill.
mTORC1
GF connect
Adhesion
EMT
Apoptosis
DNA Fragmentation
MAPK signaling
basal AKT signaling
NF-κB activity
Src activity
(nodes not shown)
Mesenchymal
Anoikis
Survival
synchronous update steps

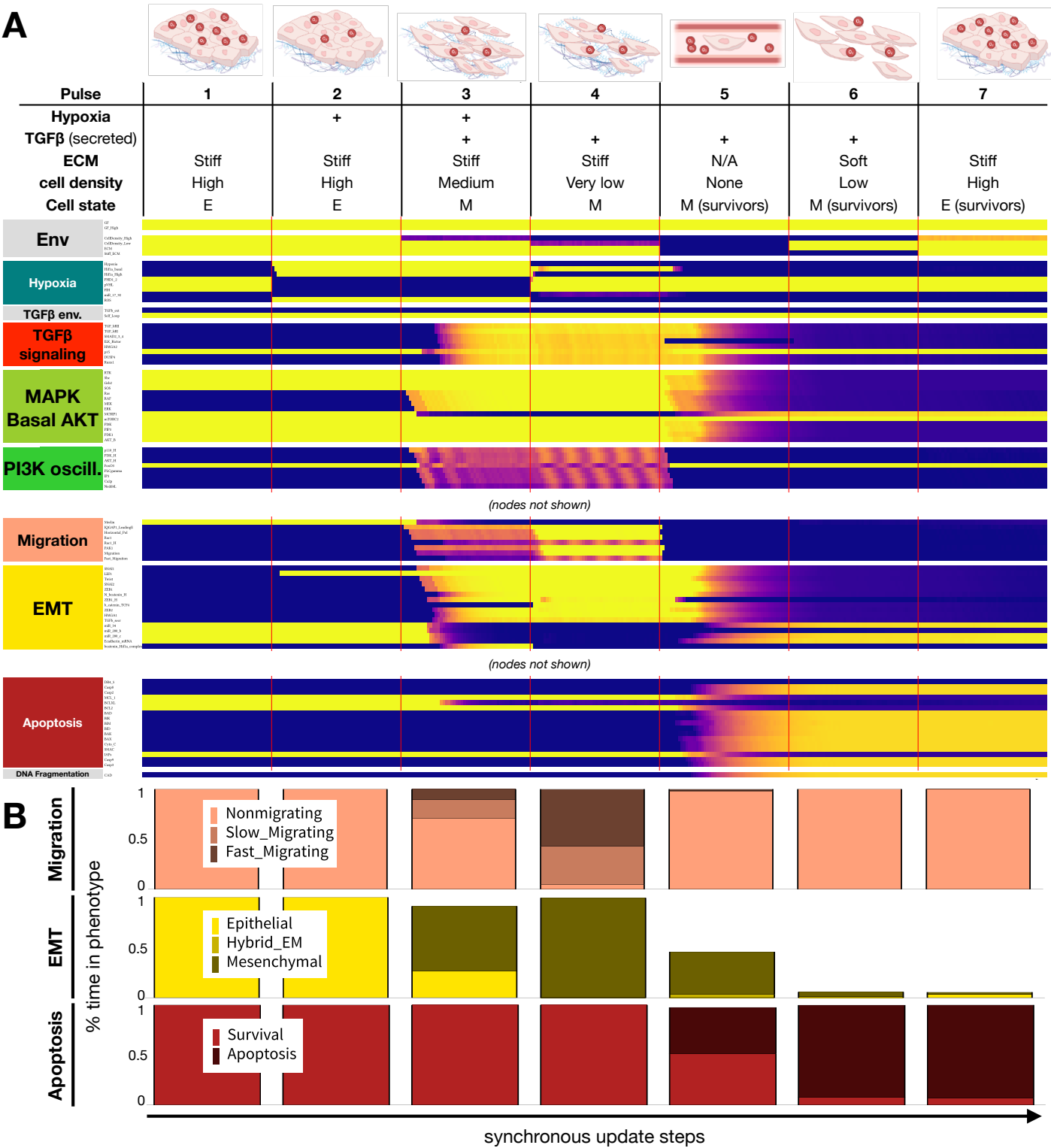
A
Pulse
1
2
3
4
5
6
7
Hypoxia
+
+
TGFβ (secreted)
+
+
+
ECM
Stiff
Stiff
Stiff
Stiff
N/A
Soft
Stiff
cell density
High
High
Medium
Very low
None
Low
High
Cell state
E
E
M
M
M (survivors)
M (survivors)
E (survivors)
Env
Hypoxia
TGFβ env.
TGFβ signaling
MAPK Basal AKT
PI3K oscill.
(nodes not shown)
Migration
EMT
(nodes not shown)
Apoptosis
DNA Fragmentation
B
Migration
Nonmigrating
Slow_Migrating
Fast_Migrating
EMT
Epithelial
Hybrid_EM
Mesenchymal
Apoptosis
Survival
Apoptosis
% time in phenotype
1
0.5
0
synchronous update steps